Science of the Total Environment 756 (2021) 144051

Contents lists available at ScienceDirect

Science of the Total Environment

journal homepage: www.elsevier.com/locate/scitotenv

Precipitation-optimised targeting of nitrogen fertilisers in a model maize cropping system

D.M. McKay Fletcher [a,1], S.A. Ruiz [a,1], T. Dias [a], D.R. Chadwick [b], D.L. Jones [b,c], T. Roose [a,*]

[a] Bioengineering Sciences Research Group, Department of Mechanical Engineering, School of Engineering, Faculty of Engineering and Physical Sciences, University of Southampton, SO17 1BJ, UK
[b] School of Natural Science, Environment Centre Wales, Bangor University, Bangor, Gwynedd LL57 2UW, UK
[c] SoilsWest, UWA School of Agriculture and Environment, The University of Western Australia, Perth, WA 6009, Australia

HIGHLIGHTS

- Optimising N fertilisation strategies for uncertain precipitation climates was investigated.
- Study considers optimal fertilisation applications (hydro/anthropo/bio/lithosphere).
- Coupled model is used to optimise N use by crops considering stochastic rainfall patterns.
- N use is suboptimal in wet conditions due to leaching and in dry conditions due to low mobility.
- Best crop N use is achievable under dry conditions but requires more accurate application times.

GRAPHICAL ABSTRACT

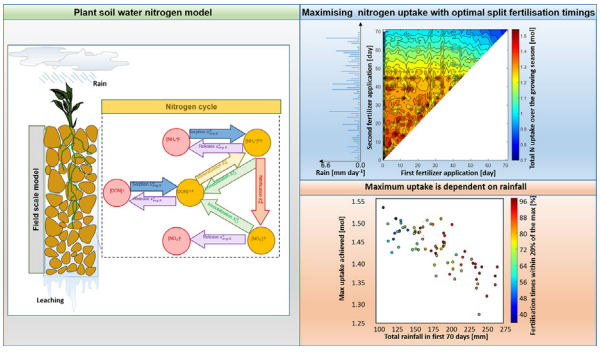
Plant soil water nitrogen model
Rain
Nitrogen cycle
Field scale model
Leaching
Maximising nitrogen uptake with optimal split fertilisation timings
Second fertilizer application [day]
First fertilizer application [day]
Rain [mm day⁻¹]
Total N uptake over the growing season [mm]
Maximum uptake is dependent on rainfall
Max uptake achieved [mol]
Total rainfall in first 70 days [mm]
Fertilization times within 20% of the max [%]

ARTICLE INFO

Article history:
Received 8 September 2020
Received in revised form 19 November 2020
Accepted 19 November 2020
Available online 24 November 2020

Editor: Fernando A.L. Pacheco

Keywords:
Fertiliser optimisation
Sustainable agroecosystems
Greenhouse gases
Climate modelling
Nutrient use efficiency

ABSTRACT

Typically, half of the nitrogen (N) fertiliser applied to agricultural fields is lost to the wider environment. This inefficiency is driven by soil processes such as denitrification, volatilisation, surface run-off and leaching. Rainfall plays an important role in regulating these processes, ultimately governing when and where N fertiliser moves in soil and its susceptibility to gaseous loss. The interaction between rainfall, plant N uptake and N losses, however, remains poorly understood. In this study we use numerical modelling to predict the optimal N fertilisation strategy with respect to rainfall patterns and offer mechanistic explanations to the resultant differences in optimal times of fertiliser application.

We developed a modelling framework that describes water and N transport in soil over a growing season and assesses nitrogen use efficiency (NUE) of split fertilisations within the context of different rainfall patterns. We used ninety rainfall patterns to determine their impact on optimal N fertilisation times. We considered the effects of root growth, root N uptake, microbial transformation of N and the effect of soil water saturation and flow on N movement in the soil profile. On average, we show that weather-optimised fertilisation strategies could improve crop N uptake by 20% compared to the mean uptake. In drier years, weather-optimising N applications improved the efficiency of crop N recovery by 35%. Further analysis shows that maximum plant N uptake is greatest under drier conditions due to reduced leaching, but it is harder to find the maximum due to low N mobility. The model could capture contrasting trends in NUE seen in previous arable cropping field trials. Furthermore, the model

* Corresponding author at: Bioengineering Sciences Research Group, Department of Mechanical Engineering, School of Engineering, Faculty of Engineering and Physical Sciences, University of Southampton, University Road, Southampton SO17 1BJ, UK.
E-mail address: T.Roose@soton.ac.uk (T. Roose).
[1] Both authors contributed equally.

https://doi.org/10.1016/j.scitotenv.2020.144051
0048-9697/© 2020 Elsevier B.V. All rights reserved.

predicted that the variability in NUE seen in the field could be associated with precipitation-driven differences in N leaching and mobility. In conclusion, our results show that NUE in cropping systems could be significantly enhanced by synchronising fertiliser timings with both crop N demand and local weather patterns.
© 2020 Elsevier B.V. All rights reserved.

1. Introduction

Over 50% of global food production relies on synthetic nitrogen (N) fertilisers (Erisman et al., 2008). N is a key macronutrient for crop growth, playing a crucial role in plant metabolic processes and is a vital component for developing plant structures (Barber, 1995). In agriculture, N availability is one of the primary factors limiting crop yield (Zhao et al., 2005). Global application of N fertiliser has increased from 4 to 83 teragrams per year from 1950 to 2000 and is expected to exceed 100 teragrams per year by 2050 (Bouwman et al., 2013). This has led to rapid ozone depletion due the unintentional release of harmful gasses (Kinzig and Socolow, 1994) and increased aquatic and terrestrial eutrophication (Erisman et al., 2013). A large proportion of N used as fertilisers is synthesised *via* an energy intensive chemical process accounting for 1.2% of the total global primary energy production (Bicer et al., 2017). As ~40% of applied N is denitrified back into the atmosphere (Galloway et al., 2004), it is necessary to develop more efficient fertilisation strategies that optimise plant uptake while minimising N losses (*i.e.* enhance N use efficiency, NUE).

There are growing concerns that climate change will diminish the efficacy of current agricultural practices that improve NUE (Bowles et al., 2018). The '4Rs' principle ('right source, at the right rate, at the right time, in the right place') is often used when discussing strategies for NUE improvements (Snyder et al., 2014; Zhang et al., 2015). However, the practices and technology depend on the individual farm climate, soil and crop (Zhang et al., 2015). The uncertainty associated with climate change further exacerbates difficulties associated with the prognosis of suitable agricultural strategies. More in-depth analysis on climate models has demonstrated that at the local scale, dry regions are expected to remain dry while wet regions could become either wetter or drier (Roderick et al., 2014). Given these uncertainties, assessments of the factors affecting N fertilisation under both wet and dry conditions are pertinent for adequately outlining optimal N fertilisation strategies. Robertson and Vitousek (2009) argued that the mistiming of soil N availability relative to plant demand could be a primary contributor to poor NUE in annual cropping systems; further understanding of N dynamics in soil will therefore help in the design of agronomic strategies that minimise N losses.

Rainfall and soil moisture play an important role in soil N dynamics and hence NUE (Goulding, 2000). However, several studies have reported conflicting results regarding the role of soil moisture on NUE. N mobility increases with moisture, which is said to improve NUE (Gauer et al., 1992; Marshall et al., 1996). Low soil moisture can cause water stress in crops, reducing N uptake (Naser et al., 2020). Furthermore, low moisture content can reduce water connectivity in the pore space thereby limiting the region of soil accessible to the plant for N uptake. On the other hand, high rainfall flushes water through the soil, carrying N along with it (Cameron et al., 2013; Di et al., 1999; Goss et al., 1993; Powlson et al., 1992; Stout et al., 2000). Leaching rates of N depend on both soil and crop type. For example, the mobility of ammonium in soil is reduced due to it tendency to adsorb to soil surfaces, while nitrate is typically more mobile as it rarely binds in temperate soils (Tinker and Nye, 2000). Additionally, reduced oxygen availability due to high soil saturation accompanied by warm weather can enhance soil conditions for the production and emission of harmful greenhouse gases such as nitrous oxide (N_2O) (Bowles et al., 2018; Dobbie and Smith, 2001). Current tillage practices are tending towards intensification of land use through use of heavier machines (Keller et al., 2017). Soil compaction is becoming a critical issue that is impacting up to 68 million ha of arable land globally (up to 5%) (Keller et al., 2017). In this case, soil pore space is reduced which has a profound impact on water movement in soil thus compaction also affects N transport.

Studies regarding the effect of rainfall and soil moisture on NUE fall into the following categories: Low soil moisture decreases N mobility limiting plant growth resulting in lower N uptake, or, high rainfall causes excess drainage resulting in leaching. While, many studies have investigated the effects of precipitation (Li et al., 2020), it remains unclear exactly what fertilisation timings, precipitation patterns, and soil conditions result in good NUE. We aim to evaluate theoretical optimal fertilisation timings over a maize growing season for a different rainfall patterns to elucidate some the mechanisms associated with soil moisture that regulate NUE.

Previous studies have attempted to use models to understand N dynamics in soil under different climate and management scenarios. For example NCSOIL (Molina et al., 1983), ANIMO (Berghuijs-Van Dijk et al., 1985), (Smith et al., 1996), and AgriFlux (Larocque and Banton, 1995) are all models that have been developed to consider N dynamics in agricultural settings. The large drawback of these models is the consideration of discrete pools for N transformations which fail to adequately resolve soil spatially. Thus, these models cannot properly account for the spatial and dynamic interactions between soil structure, water and N transport, and root-soil interactions at sufficient spatial or temporal resolutions necessary to infer optimal fertilisation times, nor highlight sources of inefficiencies associated with hydrodynamics. While models such as STICS (Brisson et al., 2003) provide some spatial resolution, the partitioning grid size on the order of 1 cm is still relatively coarse when dealing with fluid flow in porous media. Furthermore, soil water transport processes are regulated by a semi empirical method of a 'tipping bucket' approach. It is unclear in the STICS model how N transport is coupled to water flow in the soil, if at all. The effect of water flow on N transport is an important process when considering rainfall and NUE. For these reasons, we opt to develop and use a model where soil water flow and N transport are rigorously coupled in a modelling framework that facilitates control over grid resolution, precipitation patterns and fertilisation timings.

In this paper we consider the 'at the right time' principle in the '4Rs' of reducing N loss by considering varying rainfall patterns, within an otherwise controlled model cropping system (maize). We constructed a field scale model to describe simultaneous water movement, N transport, root growth and N uptake. The model incorporates several different N species within the soil in multiple states and their associated interactions. Ninety different rainfall patterns were stochastically generated and used to understand the impact of variable precipitation patterns and fertilisation timings on N uptake. Enhanced nitrous oxide release periods were estimated implicitly to determine if optimal fertilisation timings co-locate with suboptimal enhanced greenhouse gas release. The results of the model are then compared to two previous field studies with contrasting results regarding NUE and rainfall.

2. Methods

2.1. Model overview

Our study implements a coupled field scale 1D soil water and N transport model considering growing maize roots in 1 m^3 of soil (Fig. 1a). The model considers soil water dynamics across a spatially resolved depth of 1 m. Water movement through the soil is described using Richards' equation (Richards, 1931) (Fig. 1b). N species are

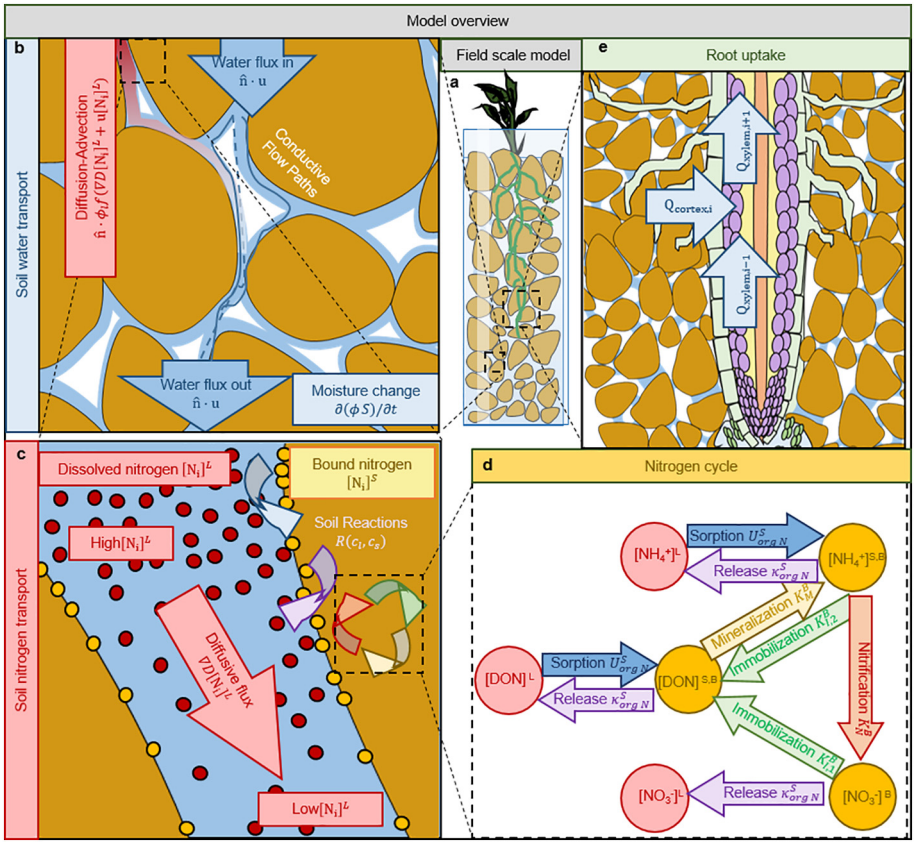

Fig. 1. Overall model description. **a** presents a coupled field scale model of a growing plant root through a spatially resolved 1D soil domain. **b**, The soil domain is considered to be partially saturated and described by Richards' equation. **c**, Nitrogen is transported *via* advection-diffusion in the water filled pore space. Nitrogen species interact with soil particle surfaces *via* sorption and release. **d**, Once bound to surfaces the nitrogen cycle considered in the model. The reactions are reported alongside the reaction constants involved. The K_i^B constants represent the Michaelis-Menten constants for the different reactions promoted by the microbial community, *i.e.*, nitrification (K_N^B), mineralisation (K_M^B) and immobilisation of nitrate ($K_{I,2}^B$) and ammonium ($K_{I,1}^B$). The constants U_i^S represent the rate of sorption to the mineral surfaces occurring in the absence of microorganisms, and the constants κ_i^S represent the linear release rates from the mineral surfaces. **e**, Growing maize roots act as a sink term for water and nitrogen species.

considered to diffuse in the soil pore water, move *via* advection with the volumetric water fluxes and interact with soil mineral surfaces (Fig. 1c). N reactions are regulated by a conceptual N-cycle model incorporating bound and dissolved NO_3^-, NH_4^+, and dissolved organic N (DON) (Fig. 1d) (Ruiz et al., 2020a). The model considers root growth and root water and N uptake (Fig. 1d) in a 1 m^3 region of soil containing four maize plants, represented by one space dimension with time and space dependent root length densities. The 1D approximation implicitly assumes symmetric conditions across the other spatial dimensions, and neglects explicit effects of 2D or 3D geometric heterogeneities in order to focus on optimising fertilisation processes at field scales. It is worth noting that the 1D reduction can be implemented with minimal divergence from 3D results for root water uptake (Daly et al., 2018). As the model is coupled, the root water uptake influences the transport of N in solution that could subsequently be taken up by the plant roots.

As model boundary inputs, stochastically generated rainfall supplies the soil with water from the top. Temperature is assumed to be constant to focus on the effect of changing rainfall patterns only. Nitrate fertiliser is applied at two time points to the soil surface representing split fertiliser application. At the bottom boundary, water is considered to drain freely at a depth of 1 m. Similarly, dissolved N species are considered to flow out of the domain with the water (*i.e.* leached N).

For the growing maize roots, we assume a constant (negative) xylem pressure at the top of the root system induced by transpiration. This pressure serves as a boundary condition to determine xylem pressure as a function of depth (Roose and Fowler, 2004; Ruiz et al., 2020b). Root N acquisition is governed by Michaelis-Menten kinetics (Tinker and Nye, 2000).

The model was used to estimate optimal fertilisation strategies for maximising root N uptake (and thereby minimise leaching) while implicitly considering the system's susceptibility to N_2O production. Simulations were exhaustively carried out for a collection of rainfall scenarios and fertilisation application times. For each generated rainfall pattern (90 generated and one mean), the simulation was solved for each possible fertilisation time (daily resolution) and total plant N uptake and susceptibility to transformation to N_2O were calculated. The simulations were solved for 112 days to be representative of a growing season. The fertilisation times, t_1 and t_2 were always less than 70 days post germination, which includes typical fertilisation timings for maize production in temperate climates from early to mid-season (Roques et al., 2016; Walsh et al., 2012). The first application only contained 0.33 mol of nitrate, while the second application contained 0.67 mol of nitrate. In total, 1 mol of nitrate was added to the system, equivalent to 144 kg ha^{-1} representative of the typical amount that maximises maize yields while reducing N losses (Goulding, 2000). Simulations were solved on the IRIDIS 4 supercomputing cluster along with several desktop computers. The model was run for over 400,000 realisations.

2.2. Water movement model

Consider a $1 \times 1 \times 1$ m^3 region of soil represented in one dimension by a depth of 1 m. For water movement in soil, Richards' equation was used (Bear, 2012). Richards' equation is derived by combining the equation for mass balance of soil water flow (Richards, 1931),

$$\phi\frac{\partial S}{\partial t}+\nabla\cdot\mathrm{u}=-F_{\mathrm{W}},0\le x_3\le 1, \tag{1}$$

with Darcy's law,

$$\mathrm{u}=-\frac{\kappa(S)}{\mu}(\nabla p+\rho g),0\le x_3\le 1. \tag{2}$$

The result is Richards' equation in a mixed form,

$$\phi\frac{\partial S}{\partial t}+\nabla\cdot\left[-\frac{\kappa(S)}{\mu}(\nabla p+\rho g\hat{\mathrm{e}}_3)\right]=-F_{\mathrm{W}},0\le x_3\le 1, \tag{3}$$

where ϕ [m^3_{pore} m^{-3}_{bulk}] is the soil porosity, S is the relative saturation (*i.e.* $S=\phi_l/\phi$, where ϕ_l [m^3_{water} m^{-3}_{bulk}] is the volumetric water content), u [m^3_{water} $m^{-2}_{surface}$ s^{-1}] is the volume flux of water, $\hat{\mathrm{e}}_3$ is the unit vector vertically upwards, $\kappa(S)$[m^2_{water}] is the relative hydraulic permeability, μ [Pa s] is the viscosity of water, p [Pa] is the soil capillary pressure, ρ [kg_{water} m^{-3}_{water}] is the density of water, g [m s^{-2}] is the acceleration due to gravity and F_W[m^3_{water} m^{-3}_{bulk} s^{-1}] is a sink term which describes water uptake *via* plant roots; this is described in the following section of the paper.

Eq. (3) is one equation for two unknowns, saturation (S) and capillary pressure (p), but S can be linked to p [Pa] using the van Genuchten water retention relation (van Genuchten, 1980),

$$S(p)=\left[\left(\frac{p_{\mathrm{a}}-p}{p_{\mathrm{c}}}\right)^{\frac{1}{1-m}}+1\right]^{-m}, \tag{4}$$

where p_a [Pa] is the atmospheric pressure, p_c [Pa] is the characteristic suction pressure and m is a van Genuchten parameter. The parameters p_c [Pa] and m are determined experimentally for each soil (van Genuchten, 1980), but can also be estimated using computational techniques based on X-ray CT imaging of soil (Cooper et al., 2017). We note that the van Genuchten function is a continuous estimation of the cumulative soil pore size distribution (Koebernick et al., 2017). In other words, it is a continuous function that preserves the discrete structural information of the soil heterogeneity. However, information pertaining to larger biopores are likely omitted with this formulation. This is often the case due to the difficulties in measuring the hydraulic effects of macropores (Fatichi et al., 2020). We choose to set $p_a=0$, such that p is defined as the gauge pressure relative to the atmospheric pressure.

To describe the relative permeability $\kappa(S)$, we use a second van Genuchten formula (van Genuchten, 1980),

$$\kappa(S)=\kappa_{\mathrm{s}}S^{\frac{1}{2}}\left[1-\left(1-S^{\frac{1}{m}}\right)^{m}\right]^2, \tag{5}$$

where κ_s [m^2] is the saturated hydraulic permeability.

Combining Richards' Eq. (3) with the van Genuchten Eqs. (4)–(5) (van Genuchten, 1980), we can write the water movement model in terms of p only:

$$\phi\frac{\partial S(p)}{\partial p}\frac{\partial p}{\partial t}+\nabla\cdot\left\{-\frac{\kappa[S(p)]}{\mu}(\nabla p+\rho g)\right\}=-F_W, \tag{6}$$

where

$$\frac{\partial S(p)}{\partial p}=\frac{m\left[\left(\frac{-p}{p_{\mathrm{c}}}\right)^{\frac{1}{1-m}}+1\right]^{-m-1}\left(\frac{-p}{p_{\mathrm{c}}}\right)^{\frac{m}{1-m}}}{p_{\mathrm{c}}(1-m)}, \tag{7}$$

and

$$\kappa[S(p)]=\kappa_{\mathrm{s}}\left[\left(\frac{-p}{p_{\mathrm{c}}}\right)^{\frac{1}{1-m}}+1\right]^{\frac{-m}{2}}\left(1-\left\{1-\left[\left(\frac{-p}{p_{\mathrm{c}}}\right)^{\frac{1}{1-m}}+1\right]^{-1}\right\}^{m}\right)^2. \tag{8}$$

The system of Eqs. (6)–(8) completes the description of the water movement. We now describe how the growing root system is implemented and the root water uptake term, F_W.

2.3. Root growth and water uptake

The root water uptake function, F_W, is given by the difference in soil capillary pressure and the pressure inside plant roots (Roose and Fowler, 2004) and is assumed to be active only where roots are present. A planting density of four plants per m^2 is assumed (https://www.yara.co.uk/crop-nutrition/forage-maize/maize-agronomic-principals/). We consider lateral and primary roots separately. The primary root grows vertically and influences the soil water and nutrients; the lateral roots are treated as a growing length density and grow from the primary root as it enters a new region of soil. Hence we split the water uptake term, F_w into two parts, namely the primary (F^p_w) and lateral (F^l_W) root uptake such that $F_W=F^p_W+F^l_W$. The primary root water uptake is treated as a single root absorbing water in the soil

$$F^p_{\mathrm{W}}=\begin{cases}\frac{2\pi a_p k_r}{\pi(a_p+K_1\cos(\beta))^2}(p-p_r) & x_3<l_0(t)\\ 0 & x_3\ge l_0(t)\end{cases}, \tag{9}$$

where a_p [m] is the primary root radius, k_r [m Pa^{-1} s^{-1}] is the root radial conductivity per unit root length, K_1 [m] and β [rad] define the cone of influence of the primary root, p_r [Pa] is the pressure in the root xylem, and $l_0(t)$ [m] defines the depth the root has grown to by time t introduced in the following section. The lateral root water uptake is treated as growing root length density absorbing water

$$F^l_{\mathrm{W}}=\begin{cases}2\pi a_l k_r l_d(x_3,t)(p-p_r) & x_3<l_0(t)\\ 0 & x_3\ge l_0(t)\end{cases}, \tag{10}$$

where a_l [m] is the lateral root radius $l_d(x_3,t)$ [m_{root} m^{-3}_{bulk}] is a function determining the lateral root length density at depth x_3 and time t introduced in the following section.

We allow the length/depth of the primary root to change over time; this is governed by the root length $l_0(t)$ which is described after (Roose and Fowler, 2004),

$$\frac{\partial l_0(t)}{\partial t}=r\left(1-\frac{l_0(t)}{K}\right), \tag{11}$$

where r[m s^{-1}] is the initial growth rate and K[m] is the maximum root length. The lateral roots are considered as a root length density, $l_d(x_3,t)$ [m_{root} m^3_{bulk}] which start growing as the primary root reaches the given depth

$$\frac{\partial l_d(x_3,t)}{\partial t}=\begin{cases}r_d\left(1-\frac{l_d(x_3,t)}{K_d}\right) & x_3<l_0(t)\\ 0 & x_3\ge l_0(t)\end{cases}, \tag{12}$$

where K_d [m_{root} m^{-3}] is the maximum lateral root length density and r_d [m_{root} m^{-3} s^{-1}] is the initial lateral root length density growth rate (Roose et al., 2001). Notice there is a lateral root length density defined per depth of soil. Additionally, this formulation assumes primary and lateral growth is independent of external factors. Importantly, the roots will grow the same regardless of soil hydrology or soil N distribution. This assumption enables us to study water and N dynamics in isolation and attribute any differences between results to rainfall only. The temporal evolution of the lateral root length density can be seen in the Supplementary Information Fig. S6.

We describe the distribution of pressure inside the root by,

$$-k_z\frac{\partial^2 p_r}{\partial x_3^2}=2\pi a_i k_r(p-p_r)\ x_3<l_0(t), \tag{13}$$

where p_r [Pa] is the root xylem pressure as a function of the rooting system depth, k_z [$m^4\,Pa^{-1}\,s^{-1}$] is the root axial conductivity, k_r [$m\,Pa^{-1}\,s^{-1}$] is the root radial conductivity, and a_i is either the lateral or primary root radius.

2.4. Nitrogen movement and uptake model

Here we introduce a mathematical model for N movement in soil. We couple it with the water movement model derived above, thereby constructing a model for simultaneous water and N movement and plant uptake in soil. The model coupling follows the approach of (Roose and Fowler, 2004). N is a highly mobile nutrient that readily reacts and transforms in the bulk soil, thus presenting itself in a multitude of different forms regulated by the N cycle (Galloway et al., 2004). We consider N to exist in three different species, these being ammonium NH_4^+, nitrate NO_3^- and dissolved organic N (DON). These N species can exist in one or multiple states (specific to each species): either adsorbed to the soil surface and governed by adsorption/desorption reactions (denoted with subscript *S*), mediated by microbial reactions (denoted with subscript *B*) and in the soil pore water (denoted with subscript *L*). As the soil microbiota are typically located on soil mineral surfaces we effectively treat soil sorbed and microbial governed N species as the same pool (denoted superscript *S*, *B*), however, we keep track of the specific state of the N species to remind readers when reactions are mediated by microbes. Fig. 1d shows a map of the reactions between different N species and the states each species exists in. Further details of the N cycle and the model derivation and assumptions are presented in Ruiz et al. (2020a).

The N species nitrate NO_3^- can exist within the microbes within the soil, which instigate reactions affecting nitrate. These reactions can be represented mathematically by,

$$\frac{d[NO_3^-]^B}{dt} = \left(\frac{V_{max}}{K_N^B + [NH_4^+]^{S,B}}\right)[NH_4^+]^{S,B} - \left(\left(\frac{\frac{1}{2}V_{max}}{K_{I,2}^B + [NO_3^-]^B}\right) + \kappa_{NO_3}^S\right)[NO_3^-]^B, \quad (14)$$

where $[NO_3^-]^B$ [mol m_{solid}^{-2}] is nitrate associated with microbes, $[NH_4^+]^{S,B}$ [mol m_{solid}^{-2}] is ammonium sorbed to soil surfaces and associated with microbes, V_{max} [mol s^{-1}] is the maximum sorption rate, K_N^B [mol m_{solid}^{-2}] is the concentration of $[NH_4^+]^{S,B}$ when the nitrification reaction rate is half V_{max}, $K_{I,2}^B$ [mol m_{solid}^{-2}] is the concentration of $[NO_3^-]^B$ when the immobilisation reaction rate is a quarter V_{max} and κ_{NO3}^S[s^{-1}] is the linear release reaction rate from $[NO_3^-]^B$ to $[NO_3^-]^L$ (Ruiz et al., 2020a).

The N species ammonium NH_4^+ and DON can exist in the sorbed form, *i.e.*, absorbed onto the soil mineral surfaces and associated with microbes. We represent these two species mathematically by

$$\frac{d[DON]^{S,B}}{dt} = \left(\frac{V_{max}}{K_{I,1}^B + [NH_4^+]^{S,B}}\right)[NH_4^+]^{S,B} + \left(\frac{\frac{1}{2}V_{max}}{K_{I,2}^B + [NO_3^-]^B}\right)[NO_3^-]^B - \left(\left(\frac{V_{max}}{K_M^B + [DON]^{S,B}}\right) + \kappa_{org\,N}^S\right)[DON]^{S,B} + U_{org\,N}^S[DON]^L, \quad (15)$$

$$\frac{d[NH_4^+]^{S,B}}{dt} = -\left(\left(\frac{V_{max}}{K_N^B + [NH_4^+]^{S,B}}\right) + \left(\frac{V_{max}}{K_{I,1}^B + [NH_4^+]^{S,B}}\right) + \kappa_{NH_4}^S\right)[NH_4^+]^{S,B} + \left(\frac{V_{max}}{K_M^B + [DON]^{S,B}}\right)[DON]^{S,B} + U_{NH_4}^S[NH_4^+]^L, \quad (16)$$

where $[DON]^{S,B}$ [mol m_{solid}^{-2}] is the concentration of organic N associated with microbes and on the soil particles, $[DON]^L$ [mol m_{water}^{-3}] is the concentration of DON in soil solution, $[NH_4^+]^L$ [mol m_{water}^{-3}] is the concentration of ammonium in the soil solution, $K_{I,1}^B$ [mol m_{solid}^{-2}] is the concentration of $[NH_4^+]^{S,B}$ when the immobilisation reaction from $[NH_4^+]^{S,B}$ to $[DON]_{S,B\text{ is half }Vmax,\,KM}^B$ [mol m_{solid}^{-2}] is the concentration of $[DON]^{S,B}$ when the mineralisation reaction from $[DON]^{S,B}$ to $[NH_4^+]^{S,B}$ is a quarter V_{max}, $\kappa_{org\,N}^S$ [s^{-1}] is the linear release reaction rate from $[DON]^{S,B}$ to $[DON]^L$, $U_{org\,N}^S$ [$m_{water}^3\,m_{solid}^{-2}\,s^{-1}$] is the linear sorption reaction rate from $[DON]^L$ to $[DON]^{S,B}$, κ_{NH4}^S[s^{-1}] is the linear release reaction rate from $[NH_4^+]^{S,B}$ to $[NH_4^+]^L$, and U_{NH4}^S[$m_{water}^3\,m_{solid}^{-2}\,s^{-1}$] is the linear sorption reaction rate from $[NH_4^+]^L$ to $[NH_4^+]^{S,B}$. With these equations, only ammonium and DON on the soil particle surfaces are considered, any N species held within soil particles is assumed not to have a significant effect on plant N uptake over the simulation time scale.

Eqs. (14)–(16) describe the transformation mechanisms for each of the species NO_3^-, NH_4^+ and DON when they are absorbed to the soil surfaces. To describe N movement in the pore water, we also consider the transport mechanisms diffusion and convection. The N species NH_4^+, NO_3^- and DON can exist in solution in the soil pore water. We use the bulk density of the soil, ρ_s [g m_{solid}^{-3}] and the specific surface area, a_s [$m_{solid}^2\,g^{-1}$] (Jury and Horton, 2004), to convert concentrations on the soil surfaces to concentrations in soil solution,

$$\frac{\partial}{\partial t}\left[\phi_l[NH_4^+]^L\right] + \nabla\cdot\left[-D_l\phi_l\nabla[NH_4^+]^L\right] + \nabla\cdot\left\{[NH_4^+]^L\mathbf{u}\right\} = \phi_s\rho_s a_s\left(-U_{NH_4}^S[NH_4^+]^L + \kappa_{NH_4^+}^S[NH_4^+]^{S,B}\right), \quad (17)$$

$$\frac{\partial}{\partial t}\left[\phi_l[NO_3^-]^L\right] + \nabla\cdot\left[-D_l\phi_l\nabla[NO_3^-]^L\right] + \nabla\cdot\left\{[NO_3^-]^L\mathbf{u}\right\} = \phi_s\rho_s a_s\left(\kappa_{NO_3}^S[NO_3^-]^B\right) - F\left([NO_3^-]^L\right), \quad (18)$$

$$\frac{\partial}{\partial t}\left[\phi_l[DON]^L\right] + \nabla\cdot\left[-D_l\phi_l\nabla[DON]^L\right] + \nabla\cdot\left\{[DON]^L\mathbf{u}\right\} = \phi_s\rho_s a_s\left(-U_{org\,N}^S[DON]^L + \kappa_{org\,N}^S[DON]^{S,B}\right), \quad (19)$$

where $[NO_3^-]^L$ [mol m_{water}^3] is the concentration of nitrate in pore water, ϕ_s is the volumetric proportion of soil solids and $F([NO_3^-]^L)$ is the plant nitrate uptake function. We note that with these equations the model assumes soil properties are constant in depth.

In Eqs. (17)–(19), the volumetric water content ϕ_l is related to the soil water pore pressure p by the suction characteristic $\phi_l = \phi S(p)$. In addition, we state that u is described by Darcy's law, as in the water movement model, Eq. (2). Finally, we assume D_l can be expressed by the power law,

$$D_l = D_f\phi^d S(p)^d, \quad (20)$$

where D_f [$m_{water}^2\,s^{-1}$]is the diffusion coefficient in free liquid and d [−] is the impedance factor of the solute that accounts for the tortuosity of the solute moving through the soil pore space (Nye and Tinker, 1977). We note that N-containing nanoparticles may not technically behave as ideally bound N or completely dissolved N. However, the potential colloidal transport behaviour of N-nanoparticles will be sufficiently characterised by our spatially averaged diffusion-convection transport description at field scales (Krehel et al., 2015).

As with the root water uptake, we split N uptake between primary (F^p) and lateral root (F^l) so that $F = F^p + F^l$. Only nitrate in solution is assumed to be absorbed by the plant due to the high proportion of nitrate in the model system compared to other species and it is deemed essential for plant development (Liu et al., 2014). In order to appropriately scale the influence of the primary root uptake to the field scale, we consider the matched asymptotic estimation. For the full derivation and validation of the method, see Roose et al. (2001). The resulting expression is as follows,

$$F^p\left([NO_3^-]^L\right) = \begin{cases} \dfrac{\dfrac{4\pi a_p F_m}{K_m \pi (a_p + K_1\, cos(\beta))^2}[NO_3^-]^L}{1 + \dfrac{[NO_3^-]^L}{K_m} + L(p,t) + \sqrt{4\dfrac{[NO_3^-]^L}{K_m} + \left(1 - \dfrac{[NO_3^-]^L}{K_m} + L(p,t)\right)^2}} & x_3 < l_0(t) \\ 0 & x_3 \geq l_0(t) \end{cases} \tag{21}$$

where $l_0(t)$ is the depth/length of the primary root defined in Eq. (11),

$$L(p,t) = \frac{\lambda(p)}{2}\ \ln(\alpha(p)(t - t_0) + 1), \tag{22}$$

$$\lambda(p) = \frac{F_m a_p}{D_f \phi^{d+1} S(p)^{d+1} K_m}, \tag{23}$$

and

$$\alpha(p) = \frac{4e^{-\gamma} D_f \phi^{d+1} S(p)^{d+1}}{a_p^2 b\left(1 + \frac{\phi}{b} S(p)\right)}, \tag{24}$$

where F_m [mol m_{root}^{-2} s^{-1}] is the maximum uptake rate of nitrate, K_m [mol m_{water}^{-3}] is the Michaelis-Menten parameter that corresponds to the nitrate concentration when the rate of N uptake by the plant is half of F_m, t_0 is the time when the nutrient uptake started, b [−] is the buffer power of nitrate and γ is the Euler-Mascheroni constant.

Lateral root nitrate uptake is given by

$$F^l\left([NO_3^-]^L\right) = \begin{cases} \dfrac{l_d(t, x_3)\dfrac{4\pi a_l F_m}{K_m}[NO_3^-]^L}{1 + \dfrac{[NO_3^-]^L}{K_m} + L_l(p,t) + \sqrt{4\dfrac{[NO_3^-]^L}{K_m} + \left(1 - \dfrac{[NO_3^-]^L}{K_m} + L_l(p,t)\right)^2}} & x_3 < l_0(t) \\ 0 & x_3 \geq l_0(t) \end{cases} \tag{25}$$

where $l_d(t)$ is the lateral root length density defined in Eq. (12), L_l is defined similarly to L (by exchanging a_p with a_l).

2.5. Boundary conditions

To form a complete description of the water movement and N transport model, we derive conditions that are imposed on the top and bottom of the soil to describe N application, rainfall and pressure distributions within the root structure.

2.5.1. Soil surface boundary conditions for nitrogen

The boundary conditions for the N species on the surface of the soil is governed by the application of fertiliser. Two applications of N are applied to the field over the growing season typically as nitrate. The first application is usually one third of the total nitrate (N_{tot}) [mol], the remaining two-thirds of NO_3^- is applied in the second application. This is implemented by imposing a time-dependent nitrate flux on the soil surface.

$$\hat{n}\cdot\left[-D_f \phi^{d+1} S(p)^{d+1} \nabla [N_i]^L\right] + \hat{n}\cdot\left\{-\frac{[N_i]^L \overline{\kappa[S(p)]}}{\mu}(\nabla p + \rho g \hat{e}_3)\right\} = q_i^{t_1,t_2}(t), x = 0, \tag{26}$$

where $\hat{n}$ is the unit normal vector pointing out of the domain. $[N_i]_L$ [mol m^{-3}] represents N species i in solution, $q_i^{t_1,\ t}{}_2(t)$ [mol m^{-2} s^{-1}] is the volume flux of the N species i in solution per unit soil surface area per unit time, this flux is zero for all species bar nitrate in soil solution, which takes the following functional form to account for the two application times

$$q_{NO_3^-}^{t_1,t_2}(t) = \frac{1}{3}N_{tot} \times X\ \frac{}{\sigma\sqrt{(2\pi)}}\ \exp\left(-\frac{1}{2}\left(\frac{t - t_1}{\sigma}\right)^2\right) + \frac{2}{3}N_{tot} \times X\ \frac{}{\sigma\sqrt{(2\pi)}}\ \exp\left(-\frac{1}{2}\left(\frac{t - t_2}{\sigma}\right)^2\right), \tag{27}$$

where t_1 [s] is the time of the first application, t_2 [s] is the time of the second application and $\sigma = 8$ hours is the standard deviation of the Gaussian representing the time it takes for the fertiliser to get into the soil solution. Note, the Gaussian nature of the fertiliser application means there is fertiliser flux into the soil slightly before and after the nominated times t_1 and t_2. This boundary flux for nitrate is zero for most times except at two pulses centred around t_1 and t_2 representing the two fertiliser applications and it integrates to N_{tot}.

2.5.2. Soil surface boundary conditions for water

The boundary condition on the surface of the soil describes the amount of water flowing into the soil due to rainfall

$$\hat{n}\cdot\left\{-\frac{\kappa[S(p)]}{\mu}(\nabla p + \rho g \hat{e}_3)\right\} = q_w(t), x = 0, \tag{28}$$

where q_w [m_{water}^3 $m_{surface}^{-2}$ s^{-1}] is the volume flux of water per unit soil surface area per unit time *i.e.* rate of rainfall. Note evaporation is not explicitly included in this boundary condition since we assume root water uptake and rainfall dominate evapotranspiration. In the simulations $q_w(t)$ has daily rainfall resolution and is determined by drawing from a distribution generated from daily rainfall rates in the southwest of England. The synthetic series of rainfall data was created from a dataset of observed daily total rainfall distributed by the Met Office Hadley Centre for the regions of South West England & Wales (https://www.metoffice.gov.uk/hadobs/hadukp/data/download.html). A period from 01/01/2010 to 31/12/2014, which spans 1826 full days, is used to create a cumulative density function. Current rainfall data, as opposed to predicted, is used so the results were comparable to a previous field trial (Powlson et al., 1992). For the purposes of this analysis, the function used to fit the cumulative histogram did not require all the properties of a cumulative distribution function. The data is fitted with a F probability distribution (Microsoft Excel) with two degrees of freedom. In total, 90 rainfall patterns were created from this distribution by using a random number generator from 0 to 1 (drawn uniformly) to establish the accumulated probability for a given day, which is then used to draw a daily rainfall value from the cumulative density function. This approach to sampling rainfall rates ignores seasonal variations in rainfall patterns. However, since on average every day will have a rainfall rate equal to the mean, results using variable and a constant mean rainfall rate will be directly comparable. Thus, the results allowed us to determine if using constant rainfall in N uptake models is a valid assumption.

2.5.3. Base layer boundary conditions

For the water boundary at the base of the soil domain, we set a free drainage condition

$$\hat{n}\cdot -\frac{\kappa[S(p)]}{\mu}(\nabla p + \rho g \hat{e}_3) = \hat{n}\cdot -\frac{\kappa[S(p)]}{\mu}(\rho g \hat{e}_3), x = 1. \tag{29}$$

This condition means that water can be released with the effect of gravity. This assumption implies that the water table is consistently well below the 1 m depth of soil we are considering. Thus, this model is not representative of flooded conditions.

For the N species boundary conditions, the compounds leave with the advective flux but not the diffusive,

$$\hat{n}\cdot\left[-D_f\phi^{d+1}S(p)^{d+1}\nabla[N_i]^L\right]+\hat{n}\cdot\left\{-\frac{[N_i]^L\overline{\kappa[S(p)]}}{\mu}(\nabla p+\rho g\hat{e}_3)\right\}=\hat{n}\cdot\left\{-\frac{[N_i]^L\overline{\kappa[S(p)]}}{\mu}(\nabla p+\rho g\hat{e}_3)\right\},\ x=1, \quad (30)$$

i.e. the N dissolved in the soil water leaves with water in the free drainage condition.

2.5.4. Root boundary conditions

The ordinary differential equation described in Eq. (6) describes the distribution of pressure in the roots, and hence requires boundary conditions at the top and bottom of the roots to determine a solution. At the base of the root, *i.e.* at the soil surface we prescribe a constant driving pressure,

$$p_r(x=0)=P, \quad (31)$$

where P [Pa] is the driving pressure from transpiration and $p_r(x=0)$ is the pressure inside the roots at the soil surface. This assumption implies that stomatal activity is considered constant in time in the simulations, *i.e.*, we are assuming that the temperature in the atmosphere does not vary too extremely to stop stomatal function. Similarly, we propose that the structural properties of the root tip prevent a flux, hence, we impose the no-flow condition at the root tip,

Table 1
Parameters used in the model. The possible parameter ranges used in the sensitivity analysis in the supplementary information is included as a percent difference of the model parameter. The confidence interval can be found in the supplementary information.

Parameter	Value (% change in sensitivity analysis)	Unit	Description
a_p	3×10^{-4} (−100, + 1000%)	m	Primary root radius of maize (Sharp et al., 1988)
a_l	3.2×10^{-5} (−100, +1000%)	m	Lateral root radius of maize
k_r	2.49×10^{-13}	m Pa^{-1} s^{-1}	Root radial water conductivity per (Roose and Fowler, 2004)
K_1	0.08 (±100%)	m	Typical lateral length (Roose and Fowler, 2004)
β_1	$\pi/4$	rad	Lateral branching angle (Roose and Fowler, 2004)
r	1×10^{-7} (−100, +1000%)	m s^{-1}	Initial primary root growth rate (Roose and Fowler, 2004)
K	0.5 (±100)	m	Maximum primary root length (Roose and Fowler, 2004)
r_d	0.02 (−100, +1000%)	m^2_{root} m^{-3} s^{-1}	Initial lateral root length density growth rate
K_d	1.5×10^4	m^2_{root} m^{-3}	Maximum lateral root length density
ϕ	0.4 (±100%)	m^3_{pore} m^{-3}_{bulk}	Volumetric soil porosity (van Genuchten, 1980)
μ	8.9×10^{-4}	Pa s	Viscosity of water
ρ	1000	kg m^{-3}	Density of water
g	9.81	m s^{-2}	Acceleration due to gravity
p_a	0	Pa	Pressures are relative to atmospheric pressure
p_c	23200	Pa	Characteristic suction pressure (van Genuchten, 1980)
m	0.51	–	van Genuchten parameter (van Genuchten, 1980)
κ_s	5.2×10^{-14} (±100%)	m^2	Saturated hydraulic permeability (van Genuchten, 1980)
k_z	1.19×10^{-14}	m^4 Pa^{-1} s^{-1}	Root axial conductivity
V_{max}	3.33×10^{-9}	mol s^{-1}	Maximum sorption rate for microbial driven reactions (Ruiz et al., 2020a)
K_N^B	9.4×10^{-6}	mol m^{-2}_{solid}	Concentration of $[NH_4^+]^{S,\,B}$ when the nitrification reaction rate is half V_{max} (Ruiz et al., 2020a)
$K_{I,2}^B$	9.5×10^{-4}	mol m^{-2}_{solid}	Concentration of $[NO_3^-]^B$ when the immobilisation reaction rate is quarter V_{max} (Ruiz et al., 2020a)
$\kappa_{NO_3}{}^S$	4.6×10^{-3}	s^{-1}	The linear release reaction rate from $[NO_3^-]^B$ to $[NO_3^-]^L$ (Ruiz et al., 2020a)
$K_{I,1}^B$	5.1×10^{-5}	mol m^{-2}_{solid}	Concentration of $[NH_4^+]^{S,\,B}$ when the immobilisation reaction from $[NH_4^+]^{S,\,B}$ to $[DON]_{S,\,B}$ is half V_{max} (Ruiz et al., 2020a)
K_M^B	1.5×10^{-5}	mol m^{-2}_{solid}	Concentration of $[DON]_{S,\,B}$ when the mineralisation reaction from $[DON]_{S,\,B}$to $[NH_4^+]^{S,\,B}$ is a quarter V_{max} (Ruiz et al., 2020a)
$\kappa_{org\ N}^S$	4.6×10^{-3}	s^{-1}	Linear release reaction rate from $[DON]_{S,\,B}$ to $[DON]^L$ (Ruiz et al., 2020a)
$U_{org\ N}^S$	3.7×10^{-6}	m^3_{water} m^{-2}_{solid} s^{-1}	Linear sorption reaction rate from $[DON]^L$ to $[DON]_{S,\,B}$ (Ruiz et al., 2020a)
$\kappa_{NH_4}{}^S$	4.6×10^{-3}	s^{-1}	Linear release reaction rate from $[NH_4^+]^{S,\,B}$ to $[NH_4^+]^L$ (Ruiz et al., 2020a)
$U_{NH_4}{}^S$	1.3×10^{-5}	m^3_{water} m^{-2}_{solid} s^{-1}	Linear sorption reaction rate from $[NH_4^+]^L$ to $[NH_4^+]^{S,\,B}$ (Ruiz et al., 2020a)
D_f	2×10^{-9} (−100, +1000%)	m^2 s^{-1}	Diffusion coefficient of N species in free liquid (Shackelford and Daniel, 1991)
ρ_s	2700	g m^{-3}_{solid}	Bulk density of the soil
a_s	44.4 (−100, +1000%)	m^2_{solid} g^{-1}	Specific surface area of the soil
d	2 (±100%)	–	Impedance factor to diffusion (Nye and Tinker, 1977)
F_m	1×10^{-4}	mol m^{-2}_{root} s^{-1}	Maximum root nitrate uptake
K_m	0.025	mol m^{-3}_{water}	Nitrate concentration when the rate of N uptake by the plant is half of F_m,
γ	0.577	–	The Euler-Mascheroni constant
b	1	–	Buffer power of nitrate
t_1, t_2	$0\le t_1\le t_2\le 70$ days	s	First and second application times of nitrate fertiliser
N_{tot}	1	mol	Total amount of fertiliser applied over growing season. Calculated from 144 kg ha^{-1} yr^{-1} changed to mol per m^2 (Goulding, 2000).
$q_w(t)$	From data	m^3_{water} $m^{-2}_{surface}$ s^{-1}	Time dependent rainfall rate with daily resolution
σ	8	hr	Standard deviation of fertiliser pulse
P	-2.75×10^5 (±100%)	Pa	Root pressure from transpiration (Molz, 1981; Ruiz et al., 2020b)
$[NO_3^0]^L$	0.43	mol m^{-3}_{water}	Initial nitrate in solution concentration
$[NH_4^0]^L$	0.07	mol m^{-3}_{water}	Initial ammonium in solution concentration
$[DON^0]^L$	2	mol m^{-3}_{water}	Initial organic N in solution concentration
l_0	0.05	m	Initial primary root length

$$\frac{\partial p_r}{\partial x_3} - \rho g = 0, x = l_0(t), \tag{32}$$

where $l_0(t)$ is the depth of the primary root tip described by Eq. (11). Since the root grows in time, Eq. (11) is solved at each time step to account for the change in pressure due the root length changing.

2.6. Initial conditions

The initial soil pressure was chosen as the steady state pressure if no roots are present and rainfall is constantly the mean, given by the following linear function:

$$p(x) = p_\infty(x), t = 0, 0 \le x \le 1, \tag{33}$$

where $p_\infty(x)$ is −19,825 Pa at the soil surface ($x = 0$) and linearly decays in soil depth, the parametrisation of the line was determined by solving the model to stationary state without the influence of roots using constant rainfall and determining the line of best fit:

$$p_\infty(x) = -(9825x + 19825) \tag{34}$$

We also impose a uniform initial concentration for each of the N species,

$$[\mathrm{N_i}]^L(x) = \left[\mathrm{N_i^0}\right]^L, t = 0, 0 \le x \le 1, \tag{35}$$

where $[\mathrm{N_i^0}]^L$ is the initial concentration of species i in the soil.

The soil/microbial adsorbed species were assumed to be zero initially.

$$[\mathrm{N_i}]^{S,B}(x) = 0, t = 0, 0 \le x \le 1. \tag{36}$$

Finally, we defined the initial primary root length and lateral length density of the plants to be,

$$l = l_0, l_d = 0 \; t = 0. \tag{37}$$

where $l_0 = 0.05$ m is the initial root length.

2.7. Model parameters

The solutions of the dependent variables (*e.g.* N species concentration and capillary pressure) depend on a number of parameters. In this section we detail the parameter values and their origins. Several of the model parameters depend on the soil and soil texture, for example ϕ, m, κ_s and p_c. We choose to simulate a silt loam soil, hence, we selected parameter values that are typical for this type of soil, *i.e.*, $\phi = 0.396$, $m = 0.51$, $\kappa_s = 5.2 \times 10^{-14}$ m^2 and $p_c = 23200$ Pa (van Genuchten, 1980).

Values of the diffusion coefficient of a solution in free liquid, D_f, for simple electrolytes tend to be within the range of $1 \times 10^{-9} - 3 \times 10^{-9}$ m^2 s^{-1} (Shackelford and Daniel, 1991); we used a value in the middle of this range, $D_\mathrm{f} = 2 \times 10^{-9}$ m^2 s^{-1}. The typical range of the impedance coefficient d is between 0.5 and 2 (Nye and Tinker, 1977) and was chosen as $d = 2$ to be representative of a relatively compact soil. The buffer power of nitrate used in the root uptake function, Eq. (24) was chosen as $b = 1$ (Barber, 1995).

The parameters for root geometry, a_p, a_l, β_1, K_1, r, r_D, K_d and K_d, and the water–root uptake term, F_w, k_r and P, we selected typical values for maize plants. Maize primary root radius varies between 0.2 and 0.6 mm depending on a number of factors (Sharp et al., 1988). Hence the primary root radius is assumed to be $a_p = 3 \times 10^{-4}$ m. Maize lateral root radii was estimated from unpublished X-ray computed tomography images of maize and determined to be approximately $a_l = 3.2 \times 10^{-5}$ m. Typical lateral root length and branching angle used to define the cone of influence of primary roots were taken to be $K_1 = 0.08$ m and $\beta_1 = \pi/4$ rad. The root growth parameters $r = 1 \times 10^{-7}$ m s^{-1}, $r_d = 0.02$ m$^2_\mathrm{root}$ m^{-3} s^{-1}, $K = 0.5$ m and $K_d = 1.5 \times 10^4$ m$^2_\mathrm{root}$ m^{-3} were selected so the primary root depth and lateral root length density fitted the experimental data of Jones et al. (2018). The root axial conductivity, k_z was chosen as 1.19×10^{-14} m^4 Pa^{-1} s^{-1} to be representative of primary roots (Roose and Fowler, 2004). The root radial water conductivity is chosen as $k_r = 2.49 \times 10^{-13}$ m Pa^{-1} s^{-1} (Roose and Fowler, 2004). The internal root pressure at the top of the root system was taken as $P = -2.75 \times 10^5$ Pa (Molz, 1981; Ruiz et al., 2020b). The Michaelis-Menten parameters for root nitrate uptake were chosen as $F_m = 1 \times 10^{-4}$ mol m^{-2} s^{-1} and $K_m = 0.025$ mol m$^{-3}_\mathrm{water}$ (Barber, 1995).

The parameters controlling the N cycle were chosen from the modelling study of Ruiz et al. (2020a) which used the same N cycle at the pore-scale, see Table 1. The parameters to convert from volume-surface reactions to volume-volume reactions, were taken as soil bulk density, $\rho_s = 2700$ g m$^{-3}_\mathrm{solid}$ and soil specific surface area, $a_s = 44.4$ m$^2_\mathrm{solid}$ g^{-1} (Jury and Horton, 2004). The total amount of nitrate applied as fertiliser over the two pulse times t_1 and t_2 was taken as $N_{tot} = 1$ mol, calculated from the 'economic maximum' 144 kg ha^{-1} yr^{-1} (Goulding, 2000). The initial concentrations of the N species in pore water were taken as $[\mathrm{NO_3^0}]^L = 0.43$ mol m$^{-3}_\mathrm{water}$, $[\mathrm{NH_4^0}]^L = 0.07$ mol m$^{-3}_\mathrm{water}$ and $[\mathrm{DON^0}]^L = 2$ mol m$^{-3}_\mathrm{water}$.

2.7.1. Sensitivity analysis

The numerical experiment is in itself an extensive sensitivity analysis of the rainfall pattern defined by the function $q_w(t)$ and the fertilisation timings defined by the parameters t_1 and t_2 on N uptake by maize. However, other parameters in the model can have a large effect on N uptake. To determine how inaccuracies or changes in the parameters to represent alternate crops and soil types could affect the results, a supplementary sensitivity analysis was carried out. To keep the amount of simulations to a feasible number, the fertilisation timings were fixed to day 10 ($t_1 = t_2 = 10$ days) and the rainfall function is constantly the mean rainfall rate ($q_w(t) = 2.55$ mm day^{-1}) for the sensitivity analysis. The results of the sensitivity analysis can be found in the Supplementary Information. Fig. S3 shows how changing the root growth parameters affected N uptake; the most sensitive parameters were the initial growth rates of the primary roots (r) and lateral root length density (r_d), and the maximum primary root length (K). Thus, changing crop will likely affect the results. Fig. S4 shows how changes in the soil, water and N parameters affect N uptake. The diffusion of the N species in pore water (D_f), impedance to diffusion (d) and volumetric porosity (ϕ) proved to be the most sensitive parameters. However, these parameters are typically bound by the soil type and are measured for each specific soil. Changes in the proportion of ammonium in the fertiliser produced differences in uptake within the bounds of numerical precision. Additionally, changes in the proportion of N species initially adsorbed to soil solids made little difference to the resulting uptake. However, care has to be taken when interpreting these results since the model was designed for nitrate rich conditions. See the Supplementary Information for more details on the sensitivity analysis.

2.8. Numerical experiment

The model was solved a 83700 times with varying rainfall patterns and fertilisation application times to determine the effect of nitrate fertiliser application time on N uptake and susceptibility to leaching and increased N_2O release. For each generated rainfall pattern (and mean) the simulation was solved for each possible fertilisation time (daily resolution) and total plant N uptake and N susceptible to transformation to the greenhouse gas N_2O was calculated. Other greenhouse gasses associated with agriculture (*e.g.* CH_4, CO_2) were not considered. The simulations were solved for 112 days to be representative of a growing season. The fertilisation times, t_1 and t_2 were always less then 70 days post germination, with the first application time before the second, $t_1 \le t_2$.

As N_2O was not explicitly modelled, we instead determine possible periods of N_2O gas release based on the climatic conditions. Dobbie and Smith (2001) determined that N_2O release per unit of ammonium nitrate increased non-linearly with increasing moisture content and temperature in arable land. When the volumetric water content increased from 58 to 63% and the temperature from 12 to 18 °C, N_2O release per unit of ammonium nitrate release increased by a factor of 10. Hence, as an indicator for increased susceptibility of N_2O gas we use the following heuristic: If the saturation at a given depth and time is >0.63 and the rainfall at the given time is <0.5 mm day^{-1} (indicating a sunny day) then the nitrate and ammonium in water at the given depth and time has increased susceptibility to transform into N_2O gas. Mathematically, this is expressed using the function

$$N_{gas}(x_3,t) = \begin{cases} \left[NO_3^-\right]_L(x_3,t) + \left[NH_4^+\right]^L(x_3,t), S(p(x_3,t)) \geq 0.63 \text{ and } rf(t) \leq 0.5 \text{ mm day}^{-1} \\ 0, \quad else, \end{cases} \tag{38}$$

and the total N with increased susceptibility over the season is given as

$$N_{gas}^{suscept} = \int_{t=0}^{112 \text{ days}} \int_{x_3=0}^{1 \text{ m}} N_{gas}\, dx_3 dt \tag{39}$$

where $N_{gas}^{suscept}$ [mol s] is a proxy for the time and quantity of increased N_2O gas release. Care has to be taken when interpreting results regarding the potential for N_2O production, as it is only approximated implicitly and not mechanistically modelled.

3. Results

3.1. Two approaches to averaging rainfall

The model was solved using the mean rainfall rate on each day (2.5 mm day^{-1}) for each pair of fertilisation times to determine the effect of fertilisation timing on total N uptake, Fig. 2a. In addition, the model was solved using 90 different rainfall patterns (drawn from a distribution with a mean of 2.5 mm day^{-1}) for each pair of fertilisation times to determine the effect of fertilisation timing on total N uptake (Fig. 2b), susceptibility to N_2O release (Fig. 2c) and yield-scaled emissions (Fig. 2d). Yield-scaled emissions were approximated as mole of N taken up per mole s of susceptibility to N_2O release. Uptake plots for the constant rainfall (Fig. 2a) and the ensemble average (Fig. 2b) were qualitatively similar; this suggests some utility for simplified models that use constant rainfall as an input (Roose and Fowler, 2004; Ruiz et al., 2020b). However, averaging the solutions of the 90 rainfall patterns was more representative of the 'average year' since no growing season constantly has the same rainfall rate.

The mean uptake plots provided some clear and broad insights regarding suboptimal fertilisation application times (Fig. 2a and b). If the fertiliser times were too early (<2 days after planting), the total N crop uptake was low as the roots do not have time to establish and the fertiliser moved deeper than the rooting zone (Fig. 2a and b). If

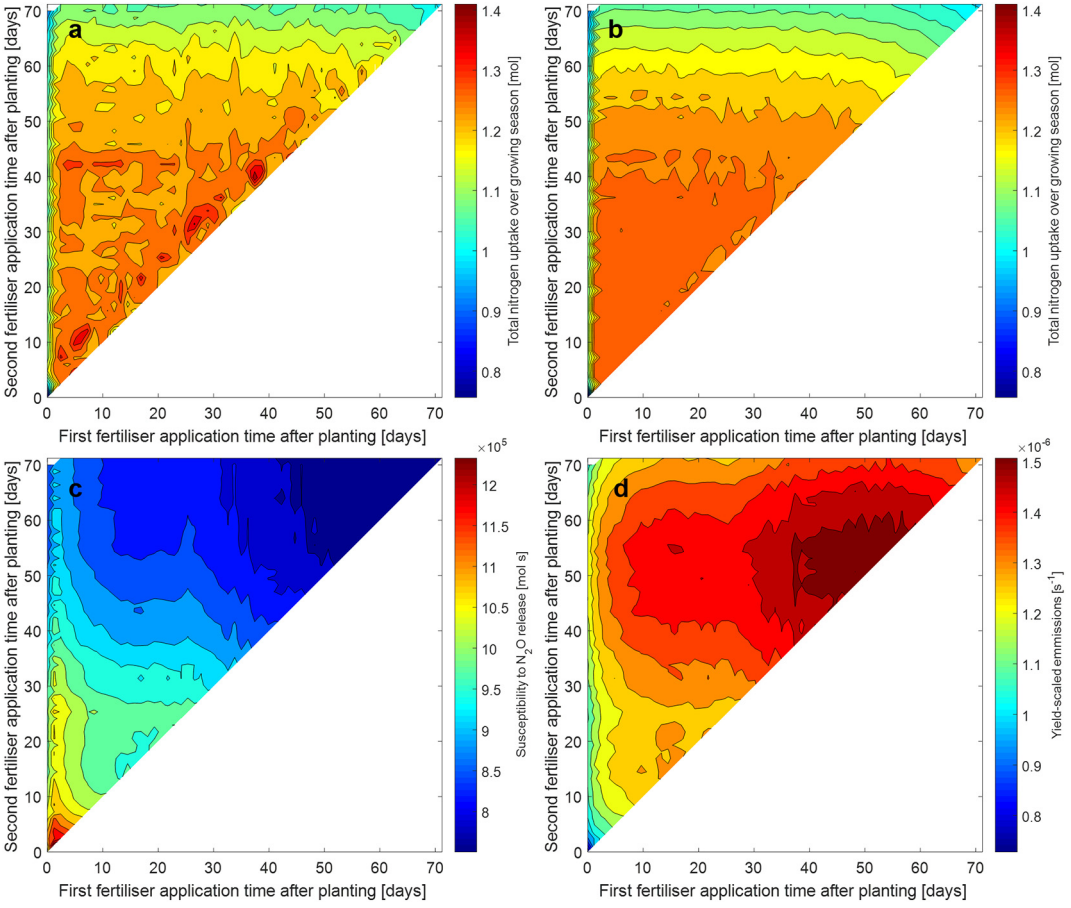

Fig. 2. Two approaches of averaging rainfall: The average impact of fertilisation times on plant nitrogen uptake and susceptibility to N_2O release. The model is solved for each pair of fertilisation times, nitrogen uptake and susceptibility to N_2O release is visualised as a heat map. **a** Nitrogen uptake when the rainfall rate is constantly the mean (2.5 mm day^{-1}). **b** Average nitrogen uptake over 90 different rainfall patterns. **c** Susceptibility to N_2O release over 90 different rainfall patterns. **d** Average yield-scaled emissions (mol of nitrogen absorbed per Susceptibility to N_2O release) over 90 different rainfall patterns. On the first fertiliser application one third and on the second two thirds of total nitrate ($N_{tot} = 1$ mol) is applied, equivalent to 144 kg ha^{-1}. The mean rainfall on each day over the 90 rainfall patterns (**c** and **d**) is approximately 2.5 mm day^{-1}.

the second fertilisation time was too late (>50 days), the uptake reduced as the plant could not take up all the fertiliser in the remaining growing season. This effect was amplified if the first application time was also late (>60 days). There were some key differences between the two averaging approaches. Most notably the maximum uptake when averaging over the 90 days was lower (1.3 mol) than when using average rainfall (1.41 mol) (Fig. 2a and b). Hence, constant rainfall is likely to over predict the "average year's" uptake. Using the optimal fertilisation times in the "average year" could improve N acquisition by 7.5% compared to the mean N uptake. More dramatic improvements could be seen if bespoke strategies were used based on precipitation patterns in individual years (20% on average), with up to 35% improvement in uptake from the mean in the drier years (elaborated in the next section). This highlights the need to find optimal N fertilisation timings in a drier climate. The uncertainty of the means shown for the ensemble average uptake (Fig. 2b) can be seen *via* the standard deviation heatmap shown in Supplementary Information Fig. S2a. Mean uptake uncertainty was minimal between second fertilisation days 40 and 60. Highest uncertainty lies during later second fertilisation days exceeding 60 days. While some uncertainties exist earlier on (prior to 40 days), they appear to be minor and more sporadic.

When mean rainfall was used, no increased susceptibility to N_2O release was observed as the constant rainfall 2.5 mm day^{-1} is above the maximum of 0.5 mm day^{-1} required to trigger our definition of increased susceptibility to N_2O release. When averaging the results over the 90 simulations, early fertilisation resulted in increased susceptibility to N_2O release (Fig. 2c). This can be attributed to the root system not having time to establish and to keep the volumetric water content below 0.63 m^3 m^{-3}.

Sustainable agricultural practices should consider greenhouse gas emissions along with plant uptake of N and yield. This can be measured by "yield-scaled emissions" defined as unit of yield per unit of greenhouse gas emissions. In the model, this was estimated by mol of N uptake per mol second of susceptibility to N_2O release, which was only defined for the ensemble average (Fig. 2d). Note that susceptibility to N_2O release was only considered implicitly in the model and was not directly calculated. There was a clear maximum when both fertilisation times were around day 50 (Fig. 2d). However, this region would not achieve maximum uptake, (Fig. 2b). The negative effects of early fertilisation were compounded using this metric, highlighting the danger of fertilisation before the roots have established.

3.2. The effect of rainfall

The maximum N uptake and susceptibility to N_2O release over all fertilisation time pairs were both calculated for each rainfall pattern and compared with the total rainfall in the first 70 days (Fig. 3a and b, respectively). To determine how likely it was to achieve close to maximum uptake/susceptibility to N_2O release, the percentage of fertilisation time pairs that achieved values within 20% of the maximum were also shown as a colour bar (Fig. 3a and b). Wetter years tended to have the lowest maximum uptakes, while dry years had the highest uptakes (Fig. 3a). However, the likelihood of achieving close to maximum uptake for wetter and most intermediate years was >75%, while in many dry years the likelihood was <60% with one only 40%. In summary, wetter years had more certain but lower maximums, drier years had less certain but higher maximums, while some intermediate years could achieve more certain high maximums, but often lower than drier years. The pattern of maximum susceptibility to N_2O release with total rainfall and likelihood was less clear (Fig. 3b). Increased N_2O release was only triggered when the soil is moist ($\phi_l > 0.63$) and when the temperature was high (determined by lack of rainfall in the model, which is only reasonable for temperate climates). Hence, increased N_2O release was triggered when a dry period follows a wet period. Thus, the pattern of rainfall, rather than the total rainfall was important for susceptibility to N_2O release. However, care has to be taken when interpreting the results regarding susceptibility to N_2O due to the implicit consideration of temperature and denitrification.

The N uptake achieved for each fertilisation time pairs for the rainfall patterns Rain 23 (a dry year, Fig. 4a), Rain 45 (a medium year, Fig. 4c) and Rain 27 (a dry year, Fig. 4e) were plotted as representative years to highlight general differences between rainfall quantities. The dry year (Fig. 4a) quickly decreased in total N uptake if the application times were too late, a feature seen when constant mean rainfall was used (Fig. 2a). However, in this case the reduction in uptake occurred with earlier fertilisation times and was more pronounced. This feature was not noticeable in the wet year Fig. 4e and was less pronounced in the medium year, Fig. 4c.

To investigate the hypothesis that low soil moisture reduces N mobility and thus uptake for dry conditions with late fertiliser applications, nitrate profiles for the dry and medium year using a late second application time ($t_1 = 9$, $t_2 = 49$ days) were shown on Fig. 5b. At day 10, a day after the first fertilisation, the nitrate peak for the medium year was

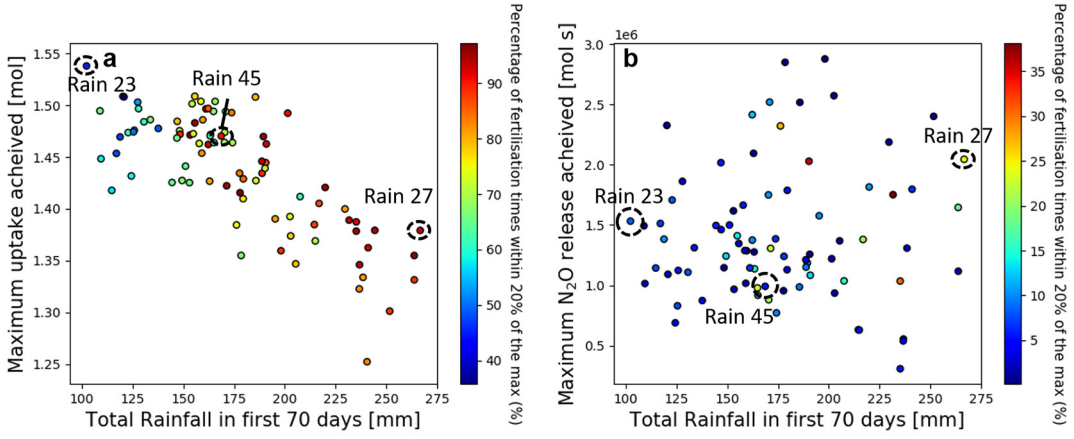

Fig. 3. Maximum uptake and susceptibility to N_2O release with likelihood. **a** The maximum crop nitrogen uptake achieved over every fertilisation time pairs *versus* total rainfall in the first 70 days for each simulated rainfall pattern. The colour bar shows the likelihood associated with the given maximum, that is, how many other fertilisation time pairs achieve at least 20% of the given maximum. The maximum uptake for Rain pattern 23 is achieved at $t_1 = 7$ and $t_2 = 14$ days; at $t_1 = 33$ and $t_2 = 37$ days for Rain pattern 45; and at $t_1 = 21$ and $t_2 = 30$ for Rain pattern 27. **b** The maximum susceptibility to N_2O release over every fertilisation time pairs *versus* total rainfall in the first 70 days for each simulated rainfall pattern. The colour bar shows the relative risk associated with the given maximum, that is, how many other fertilisation time pairs achieve at least 20% of the given maximum. The maximum susceptibility to N_2O release for Rain pattern 23 is achieved at $t_1 = 13$ and $t_2 = 27$ days; at $t_1 = 23$ and $t_2 = 23$ days for Rain 45; and at $t_1 = 21$ and $t_2 = 21$ days for Rain 27. The rainfall patterns Rain 23, 45 and 27 are chosen as representatives of a dry, medium and wet year respectively and analysed in more detail in the following figures.

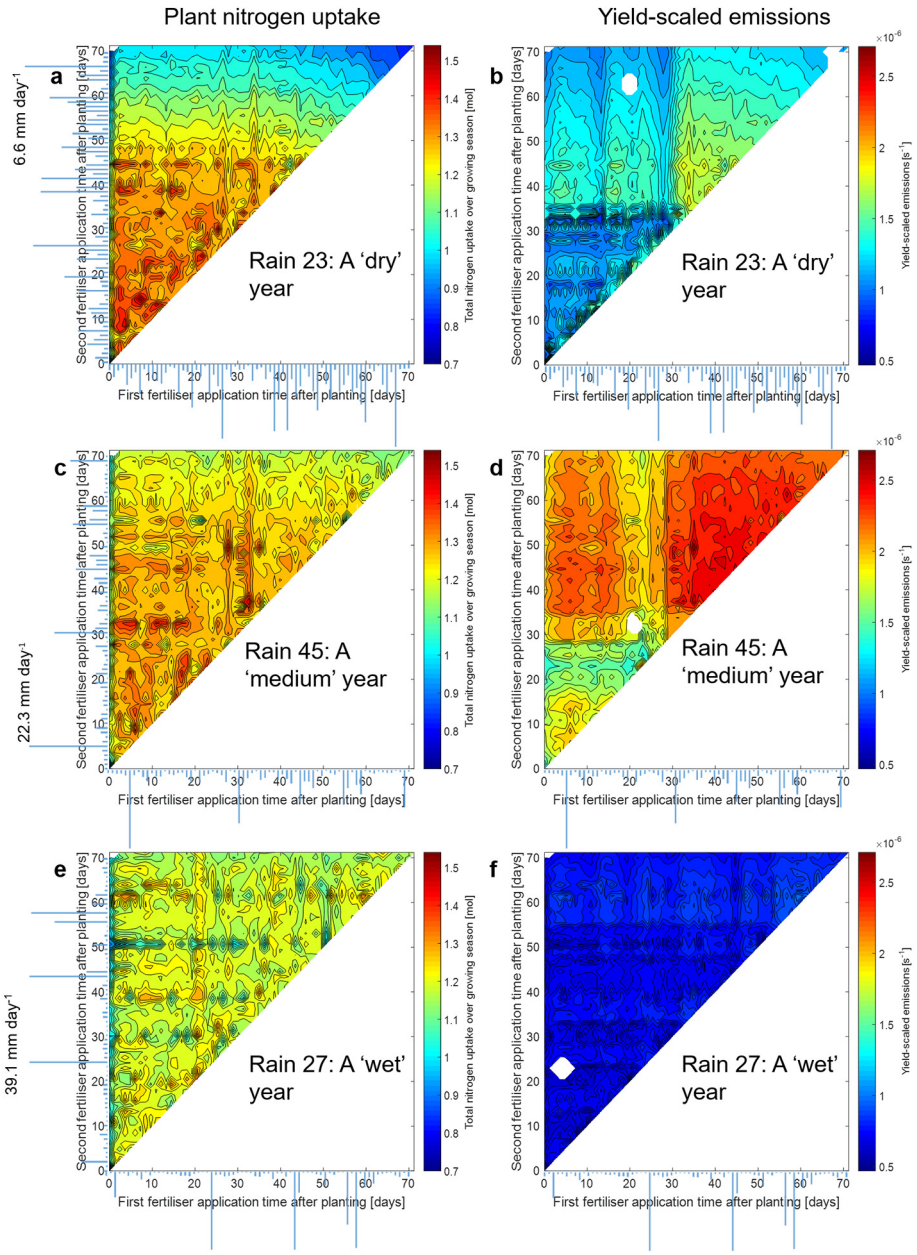

Fig. 4. Uptakes and Yield-Scaled emissions of each fertilisation time pairs for three rainfall patterns. One third and two thirds of the total applied nitrate (1 mol equivalent to 144 kg ha^{-1}) are applied at the first and second application time respectively. The rainfall rates for each day are plotted along each axis and the maximum rainfall rate is displayed for each sub figure. Note that the scales between the rainfall plots are not consistent. **a**, **c**, and **e** are heat maps showing the total nitrogen uptake over the growing season for each pair of fertilisation times for Rain pattern 23 (a 'dry' year), 45 (a 'medium' year) and 27 (a 'wet' year) respectively. **b**, **d**, and **f** show yield-scaled emissions, defined as total uptake over susceptibility to N_2O release, for Rain pattern 23 (a 'dry' year), 45 (a 'medium' year) and 27 (a 'wet' year), respectively.

slightly lower and deeper than the dry year indicating more mobility and uptake (or leaching). At day 50, a day after the second fertilisation, the N concentration peak for the dry year was distinctly narrower, higher and less deep than the peak for the medium year. By the final day, it was clear that nitrate pulse in the dry scenario had accumulated at a shallower location than the medium case, indicating lower mobility. Large narrow nitrate peaks indicate local regions of high concentration and are not efficient for uptake if the peaks are above the concentration that achieves the Michaelis-Menten maximum uptake rate, F_m, as the plant uptake rate does not exceed this rate regardless of the excess concentration.

The N uptake in the wet year was lower than both the medium and dry year for almost all fertilisation time pairs (Fig. 4a, c and e). Previous experiments suggest the decreased uptake in the wet year could be due to leaching. To test if this was the case in the model, the leaching rate for the medium and wet year are compared using their respective optimum fertilisation times (Fig. 5a). The leaching rate was higher for the wet year (Rain pattern 27) than the medium year (Rain pattern 45) for most times, confirming that leaching could be responsible for the reduced uptake in the wet year. The leaching rate in the medium year reached an early peak, higher than the wet year (Fig. 5a). This can be explained by early heavy rainfall in the medium year, see the 22.3 mm day^{-1} rate at day 5 enhancing early leaching in the medium case (Fig. 4c) while the early rainfall in the wet case was not as intense (Fig. 4e). In this case, the leachate represented N initially in the soil since the fertilisation times for the medium plot are $t_1 = 32$ and $t_2 = 37$ days. There was a risk of leaching (*i.e.* N species transporting below the 1 m domain depth) when there was early rainfall, since the root systems were not large enough to regulate the soil moisture content.

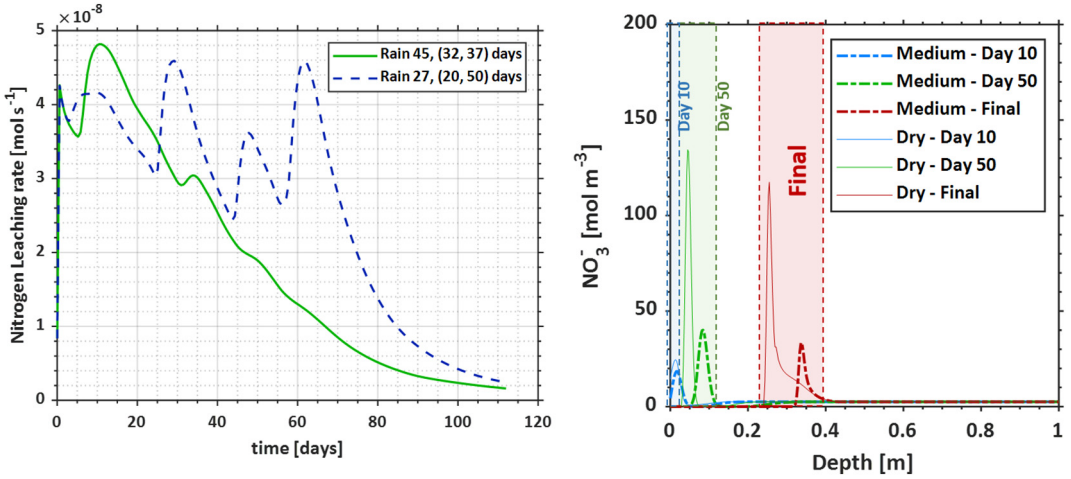

Fig. 5. Mechanisms governing nitrogen uptake and losses. **a** Nitrogen leaching rate for the 'wet' year (Rain pattern 27) with the first application at $t_1 = 20$ days and the second at $t_2 = 50$ days; and for the 'medium' year, (Rain pattern 45) with the first application at $t_1 = 32$ days and the second at $t_2 = 37$ days. These application times achieve the maximum uptake for each rainfall pattern. **b** Nitrate concentrations profiles at day 10, day 50 and at the final day 112 for the 'dry' year (Rain pattern 23) and the 'medium' year (Rain pattern 45). The fertilisation times for both years are chosen as $t_1 = 9$ days and $t_2 = 49$ days to capture the decreased uptake from late fertilisation present in the dry year but not the medium.

In some cases, rainfall within a few days of the fertilisation times seems to have a notable effect on the resulting total N uptake. For example, in the wet year, if the second application was at 50 days, low uptake was achieved for most of the first application times, indicated by a trough of low uptake rates on $t_2 = 50$ line on the heat map (Fig. 4e). Interestingly, day 50 lies between two large rainfall events. A similar trough can be seen on the $t_1 = 50$ line, although it was less pronounced since only one third of the fertiliser was used in the first application time. In the medium year, a ridge of high uptakes can be seen when the first application time is 33 days, $t_1 = 33$ days line (Fig. 4c). This fertilisation timing corresponds with a dry period following a large rainfall event. More examples like this can be seen in Fig. 4 and in more of the ninety year results not shown.

Yield-scaled emissions can be seen in Fig. 4b, d and f for the 'dry', 'medium' and 'wet' years respectively. The 'medium' had the highest yield scaled emissions (Fig. 4d), exceeding 2.5×10^{-6} [s^{-1}]. This was followed by the dry (in the order of 1.75×10^{-6} [s^{-1}]) then wet years (1×10^{-6} [s^{-1}] Fig. 4b and f). However, this pattern does not hold generally; there was no correlation between rainfall in the first 70 days and maximum (or mean) yield scaled emissions over all fertilisation time pairs. This was because susceptibility to N_2O release depends on the pattern of rainfall as opposed to just the quantity in the model. The lines at $t_1 = 30$ and $t_2 = 30$ days divide yield-scaled emissions in each year; the region defined by $t_1 < 30$, $t_2 < 30$ had the lowest yield-scaled emissions, followed by the $t_1 > 30$, $t_2 < 30$ region, while the $t_1 > 30$, $t_2 > 30$ has the highest (Fig. 4b and d, f shows the same pattern, but the colour limits hide the trend). This trend was likely an artefact of the constant root growth pattern for each simulation.

3.3. Comparison to field studies

By choosing appropriate fertilisation times, the model can recreate contrasting trends seen in long term field studies regarding NUE, Fig. 6a (increased rainfall lowered NUE) and Fig. 6b (increased rainfall increased NUE). Powlson et al. (1992) measured N loss in a number of arable fields and years in England with a spring fertilisation. They found rainfall in the 3 weeks after fertilisation could explain 73% (55% if outliers were not excluded) of the variance in the percentage of

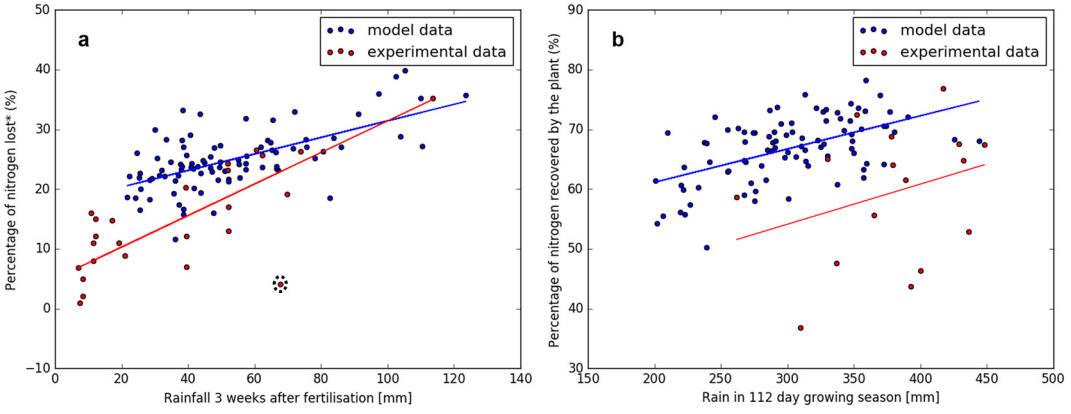

Fig. 6. Comparison of the model to field experiments. **a** The relationship between rainfall in the 3 weeks following application of nitrogen and percentage of nitrogen lost. In the model data (blue) 'loss' was defined as all nitrogen, both fertiliser and that originally in the soil, not recovered by the crop. In the model, both fertilisations were at day 5. The best fit line has a coefficient of determination $r^2 = 0.4$. The experimental data is from a field study in central England and redrawn from Powlson et al. (1992). In the experimental data (red) 'loss' was defined as isotopically labelled nitrogen applied as fertiliser (this does not include that originally in the soil) which was not recovered in the plant nor in the first 70 cm depth of soil after harvest. The best fit line has a coefficient of determination $r^2 = 0.73$. This fit excluded the outlier point highlighted with the dashed circle. If this point was included, the resulting fit produced a coefficient of determination $r^2 = 0.55$. **b** The relationship between rainfall in the growing season and the percentage of nitrogen (both in the soil and fertiliser) uptake by the plant. In the model both fertilisation times are at day 60. The best fit line has a coefficient of determination $r^2 = 0.29$. The experimental data is from a field study in the central United States and redrawn from Bowles et al. (2018); only trials with rainfall in the same range as the model were redrawn. The best fit line has a coefficient of determination $r^2 = 0.09$.

fertiliser lost (Fig. 6a), with more rainfall causing increased N loss. Our model produced a similar trend if the fertilisation times were both at 5 days post germination (fertilisation times before 24 days produced similar trends), with rainfall explaining 40% of the variance (Fig. 6a). Some of the experimental plots were geographically close and had similar rainfall (see grouping of experimental data points in rainfall in Fig. 6a), which can explain the better fit in the field experiment. Powlson et al. (1992) found that rainfall 3 weeks post fertilisation explained most of the variation in lost N. Rainfall measurements for longer or shorter periods increased the variance. In the model, 4 weeks of rainfall explained the most variation (47%). Our model mostly over predicted N loss compared to the measured losses reported by Powlson et al. (1992). This was likely due to the model including both N applied as fertiliser and N originally in the soil in the loss calculation, while the calculation in the experiment only included N from the fertiliser.

Bowles et al. (2018) collated measurements of N recovered by the crop and total rainfall in the growing season from long term field trials in the central United States (Fig. 6b). No information was given regarding fertilisation times. We suspect they were not consistent as the data is from a number of different experiments. This could explain why more variance was explained by rainfall in the model (29%) than in the data (9%) when both model fertilisation times were at 60 days. Late fertilisation match the data best in this case as increasing rainfall increased mobility and allowed the crop to absorb the fertiliser in the remainder of the growing season. This is in the sub-optimal uptake region (see $t_1 = t_2 = 60$ days in the averaged uptake plot Fig. 2b).

4. Discussion

The model captured two rainfall dependent processes important for NUE, namely that increased rainfall increases N leaching and low soil moisture decreases N mobility hindering plant uptake. The interplay between these processes was demonstrated by determining optimal fertilisation times for a number of rainfall patterns. In drier years, late application of fertiliser had a risk of low N uptake (and NUE) due to low N mobility. Low mobility caused sharp spatially localised peaks of nitrate (Fig. 5b), thus one narrow portion of the root system was responsible for acquiring the nitrate fertiliser. A greater spread of nitrate peaks would split the uptake over a larger part of the root system, improving uptake. Furthermore, persistence of large N concentrations in soil could generate cytotoxic regions that are potentially harmful to soil life (Ruiz et al., 2020a). We conclude that low mobility in the dry conditions causes the decline in nitrate uptake for late applications. A possible strategy to improve NUE in drier years is to apply the second application of fertiliser earlier or change the quantity of fertiliser applied to account for the reduced mobility and plant growth due to low water availability. Alternatively, irrigation strategies could be used. Comparing the ensemble average uptake over each of the ninety years to the simulation using constant mean (Fig. 2a and b) showed there are dangers in assuming the rainfall rate is constant when modelling N uptake. In particular, constant rainfall can over predict the "average year's" uptake.

There are crucial model assumptions to be aware of when interpreting the results. Atmospheric temperature and soil temperature were assumed to be constant. Likewise evaporative water fluxes were neglected. Varying temperatures are known to change the rates of biological processes. As the model is representative of spring to summer growing season in the UK, we assumed that the logistic root growth model captured the majority of the variations that we would see by explicitly including temperature effects. Similarly, we assumed the changes in the N cycle reaction rates due to temperature would be minimal. Additionally, we hypothesised that variations in soil moisture due to rainfall would be the important mechanism governing NUE (Powlson et al., 1992). Hence, special attention was paid to accurately describing water flow. However, in future, these assumptions should be verified by considering temperature explicitly.

The boundary condition for water flow on the base of soil domain implied that the water table was sufficiently below the 1 m depth of soil considered *i.e.* the model is not valid for flooded or waterlogged conditions (and neither is it valid in semi-arid or arid conditions). The proportion of ammonium transformed into nitrous oxide during the nitrification reaction is typically in the order of fractions of a percent (Farquharson, 2016). For this reason, it was judged to have little effect on the results regarding crop N uptake and leaching losses, and was thus omitted from the model for sake of simplicity. However, this omission prevents a truly mechanistic and quantitative assessment of nitrous oxide release. Instead a proxy for periods of increased denitrification was given using soil saturation, rainfall rates and concentrations, hence these results should be somewhat interpreted with caution.

Soil and root growth parameters were fixed during the numerical experiments, however there is variability in these parameters depending on the crop and soil type. It is likely that macro pore structures were neglected in the soil physical characterisation. We acknowledge that inclusion of this information better informs deep infiltration and groundwater recharge in wet and vegetated regions due to enhanced preferential flow (Fatichi et al., 2020). The perturbed soil physical parameters in the Supplementary Information allude to how inclusion of these features might change the simulation results (*e.g.* increased saturated hydraulic permeability, changes in soil porosity, *etc.*). However, it is worth noting that these differences are local and often become statistically insignificant when considering larger scales (Fatichi et al., 2020). Furthermore, the sensitivity analysis in the Supplementary Information shows that the root growth parameters in particular can affect the uptake measurements, hence separate simulations would be required for different crops and growth conditions. Additionally, soil properties did not change in space hence different soil sorption characteristics was not considered. These effects are better investigated using pore-scale models, which explicitly consider soil surfaces. For more details on the difference between pore-scale models and field-scale models please see Ruiz et al. (2020c).

Increased leaching was present in wetter years regardless of fertilisation times (Figs. 3a and 5a). Rainfall patterns shortly before and after fertilisation seemed to affect N uptake in the growing season in most of the ninety rainfall patterns (see Fig. 4 for examples). Additionally, the rainfall 4 weeks after application explained the most variance in N losses. This suggests that it is possible to determine fertilisation strategies based on previous and forecasted rainfall data to reduce the leaching in wet years and highlights the importance of weather prediction for agriculture improvements. The model can also be used to determine the effect of future precipitation patterns on N uptake and fertilisation times by using predicted rainfall patterns as the input data. However, it was unclear if local rainfall data (*i.e.* previous days' rain and the forecast) around fertilisation times alone can help predict the resulting N uptake. It is outside the scope of this study to test this hypothesis.

Reducing greenhouse gas emissions is also an important consideration. Although the model only implicitly considered the release of one greenhouse gas N_2O, *via* post-processing, it showed that late fertilisation can reduce its risk (Fig. 2c). Reduction of the amount of time that the fertiliser is in the soil and vulnerable to denitrification can explain this result. Nuances associated with dry, medium, and wet years highlight the potential respective severity of N_2O release on yield scaled emissions (Fig. 4). During a dry year (Fig. 4a and b), it is possible to achieve near optimal N uptake and yield scaled emissions with a second application between 40 and 45 days. Caution needs to be taken during a medium year (Fig. 4c and d), as suboptimal N uptake during late applications could still produce optimal yield scale emissions. Finally, for the wet year (Fig. 4e and f), neither varies largely with changes in fertilisation time, thus it might be feasible to consider optimising for N uptake. We note that the absolute magnitudes of N_2O emissions are not explicitly considered in this study. Future work should consider how to better incorporate the various biologically mediated reactions necessary to explicitly account for N_2O and N_2 production and emissions.

The model captured contrasting trends in NUE observed in separate field trials by choosing appropriate fertilisation timings. Namely, increased rainfall increased N loss with early fertilisation, Fig. 6a (Powlson et al., 1992) and increased rainfall increased plant N uptake with later fertilisation, Fig. 6b (Bowles et al., 2018). Variation in N uptake/loss between years in the model are similar to the two field studies, most notably Powlson et al. (1992) who's sites were from a more narrow geographical range than Bowles et al. (2018). Given that the only variation in the model is rainfall patterns it is likely that these dominate changes in N uptake/loss. However, it is likely that soil and plant properties in Powlson et al. (1992) also contribute to the variance not explained by the experimental best fit line seen in Fig. 6a. This finding is in agreement with recent reviews (Bowles et al., 2018; Greaver et al., 2016) while offering a mechanistic understanding and predictive tool for predicting the impact of changing climate. The model fertilisation timings that best match Bowles et al. (2018) were in the suboptimal range (Fig. 2). Thus, if the trends observed in the model are representative, some field trials in Bowles et al. (2018) could be fertilising too late to achieve the best N uptake (although by fertilising at day 60 they have close to optimum yield-scaled emissions, Fig. 2d). However, differences in soils, crops and rainfall patterns (as opposed to cumulative rainfall) could also explain the different experimentally observed trend with earlier fertilisation times.

In another meta-analysis of rainfall and NUE from around the world, Li et al. (2020) found that NUE increased linearly with water input until exceeding 311 mm for the growing season. From then it decreased linearly, although little of the variance was explained by these lines. This is consistent with our finding that dry years can cause poor mobility and wet years cause leaching, both resulting in poor NUE (Fig. 5). In drier years, the reduced water availability limits plant growth thereby lowering the N requirements of the crop which is often not accounted for when deciding the quantity of fertiliser to apply (Bowles et al., 2018). However, our model did not consider reduced root growth due to water shortage, which could possibly explain the less severe effect of low precipitation on NUE compared to these published meta-analyses. Our results show (and in agreement with Powlson et al. (1992)) that consideration to rainfall a few weeks post fertilisation would explain more variation in NUE in the meta-analyses of Li et al. (2020) and Bowles et al. (2018) than rainfall in the whole growing season (if the data is available). Importantly, our model suggests there is scope for improved NUE in the drier years *via* earlier fertilisation. However, crop N requirement with growth stage and water limited growth should explicitly be considered to fully understand NUE and precipitation.

Our study provides mechanistic principles that explain many of the uncertainties associated with NUE and can capture trends seen in field trials. If future climates become drier, our results suggest that it is possible to improve NUE. While under drought conditions, plant roots may penetrate deeper into the soil in order to capture water, which may lead to a decoupling between soil horizons containing fertiliser N compounds and regions with microbial life that facilitate plant N acquisition. However, under dry, but not water limited conditions, fertiliser timing would need to carefully consider forecasted rainfall patterns to achieve improved NUE. This model could be a useful tool in determining these timings. In a wetter future climate, optimised fertiliser timing only mitigates leaching marginally. Many fertiliser timings can achieve close to optimal results, thus less sophisticated strategies would be required compared to drier climates.

CRediT authorship contribution statement

D. McKay Fletcher and S.A. Ruiz – Run the simulations and wrote the manuscript. Primary contributor to the manuscript text.

T. Dias – Helped to proof read and make sure that mathematical model and physics were consistent.

D. R. Chadwick, D. L. Jones – Provided literature regarding N-cycle. Provided reliable parameterization for the model. Provided thoughtful discussion regarding modelling results.

T. Roose – Designed the study together with Chadwick and Jones. Provided feedback regarding modelling. Provided useful resources to run intensive computational studies. Revised the manuscript.

Declaration of competing interest

All authors declare no competing interest.

Acknowledgements

D.M.F., S.R. and T.R. are funded by BBSRC SARIC BB/P004180/1. T.R. is also funded by ERC Consolidator grant 646809 (Data Intensive Modelling of the Rhizosphere Processes), BBSRC SARISA BB/L025620/1. T.G.D. and T.R. are funded by EPSRC EP/M020355/1. D.L.J. and D.R.C. are supported by BBSRC SARIC BB/P004539/1 and the UK-China Virtual Joint Centre for Agricultural Nitrogen (CINAg, BB/N013468/1), which is jointly supported by the Newton Fund, *via* UK BBSRC and NERC, and the Chinese Ministry of Science and Technology.

The authors acknowledge the use of the IRIDIS High Performance Computing Facility, and associated support services at the University of Southampton, in the completion of this work.

Appendix A. Supplementary data

Supplementary data to this article can be found online at https://doi.org/10.1016/j.scitotenv.2020.144051.

References

Barber, S.A., 1995. Soil Nutrient Bioavailability: A Mechanistic Approach. John Wiley & Sons.
Bear, J., 2012. Hydraulics of Groundwater. Courier Corporation.
Berghuijs-Van Dijk, J., Rijtema, P., Roest, C., 1985. ANIMO: Agricultural Nitrogen Model. ICW.
Bicer, Y., Dincer, I., Vezina, G., Raso, F., 2017. Impact assessment and environmental evaluation of various ammonia production processes. Environ. Manag. 59, 842–855.
Bouwman, L., Goldewijk, K.K., Van Der Hoek, K.W., Beusen, A.H., Van Vuuren, D.P., Willems, J., et al., 2013. Exploring global changes in nitrogen and phosphorus cycles in agriculture induced by livestock production over the 1900–2050 period. Proc. Natl. Acad. Sci. 110, 20882–20887.
Bowles, T.M., Atallah, S.S., Campbell, E.E., Gaudin, A.C., Wieder, W.R., Grandy, A.S., 2018. Addressing agricultural nitrogen losses in a changing climate. Nature Sustainability 1, 399–408.
Brisson, N., Gary, C., Justes, E., Roche, R., Mary, B., Ripoche, D., et al., 2003. An overview of the crop model STICS. Eur. J. Agron. 18, 309–332.
Cameron, K., Di, H.J., Moir, J., 2013. Nitrogen losses from the soil/plant system: a review. Ann. Appl. Biol. 162, 145–173.
Cooper, L., Daly, K., Hallett, P., Naveed, M., Koebernick, N., Bengough, A.G., et al., 2017. Fluid flow in porous media using image-based modelling to parametrize Richards' equation. Proc. R. Soc. A. vol. 473. The Royal Society, p. 20170178.
Daly, K.R., Tracy, S.R., Crout, N.M., Mairhofer, S., Pridmore, T.P., Mooney, S.J., et al., 2018. Quantification of root water uptake in soil using X-ray computed tomography and image based modelling. Plant Cell Environ. 41 (1), 121–133.
Di, H., Cameron, K., Moore, S., Smith, N., 1999. Contributions to nitrogen leaching and pasture uptake by autumn-applied dairy effluent and ammonium fertilizer labeled with 15 N isotope. Plant Soil 210, 189–198.
Dobbie, K., Smith, K., 2001. The effects of temperature, water-filled pore space and land use on N2O emissions from an imperfectly drained gleysol. Eur. J. Soil Sci. 52, 667–673.
Erisman, J.W., Sutton, M.A., Galloway, J., Klimont, Z., Winiwarter, W., 2008. How a century of ammonia synthesis changed the world. Nat. Geosci. 1, 636–639.
Erisman, J.W., Galloway, J.N., Seitzinger, S., Bleeker, A., Dise, N.B., Petrescu, A.R., et al., 2013. Consequences of human modification of the global nitrogen cycle. Philos. Trans. R. Soc. B 368, 20130116.
Farquharson, R., 2016. Nitrification rates and associated nitrous oxide emissions from agricultural soils–a synopsis. Soil Research 54, 469–480.
Fatichi, S., Or, D., Walko, R., Vereecken, H., Young, M.H., Ghezzehei, T.A., et al., 2020. Soil structure is an important omission in earth system models. Nat. Commun. 11, 1–11.
Galloway, J.N., Dentener, F.J., Capone, D.G., Boyer, E.W., Howarth, R.W., Seitzinger, S.P., et al., 2004. Nitrogen cycles: past, present, and future. Biogeochemistry 70, 153–226.
Gauer, L., Grant, C., Bailey, L., Gehl, D., 1992. Effects of nitrogen fertilization on grain protein content, nitrogen uptake, and nitrogen use efficiency of six spring wheat (Triticum aestivum L.) cultivars, in relation to estimated moisture supply. Can. J. Plant Sci. 72, 235–241.

Goss, M., Howse, K., Lane, P., Christian, D., Harris, G., 1993. Losses of nitrate-nitrogen in water draining from under autumn-sown crops established by direct drilling or mouldboard ploughing. J. Soil Sci. 44, 35–48.
Goulding, K., 2000. Nitrate leaching from arable and horticultural land. Soil Use Manag. 16, 145–151.
Greaver, T., Clark, C., Compton, J., Vallano, D., Talhelm, A., Weaver, C., et al., 2016. Key ecological responses to nitrogen are altered by climate change. Nat. Clim. Chang. 6, 836–843.
Jones, D., Magthab, E., Gleeson, D., Hill, P., Sánchez-Rodríguez, A., Roberts, P., et al., 2018. Microbial competition for nitrogen and carbon is as intense in the subsoil as in the topsoil. Soil Biol. Biochem. 117, 72–82.
Jury, W.A., Horton, R., 2004. Soil Physics. John Wiley & Sons.
Keller, T., Colombi, T., Ruiz, S., Manalili, M.P., Rek, J., Stadelmann, V., et al., 2017. Long-term soil structure observatory for monitoring post-compaction evolution of soil structure. Vadose Zone J. 16, 1–16.
Kinzig, A.P., Socolow, R.H., 1994. Human impacts on the nitrogen cycle. Phys. Today 47, 24–31.
Koebernick, N., Daly, K.R., Keyes, S.D., George, T.S., Brown, L.K., Raffan, A., et al., 2017. High-resolution synchrotron imaging shows that root hairs influence rhizosphere soil structure formation. New Phytol. 216, 124–135.
Krehel, O., Muntean, A., Knabner, P., 2015. Multiscale modeling of colloidal dynamics in porous media including aggregation and deposition. Adv. Water Resour. 86, 209–216.
Larocque, M., Banton, O., 1995. Gestion de la contamination des eaux souterraines par les fertilisants agricoles: application du modèle AgriFlux. Revue des sciences de l'eau/Journal of Water Science 8, 3–20.
Li, Y., Cui, S., Zhang, Z., Zhuang, K., Wang, Z., Zhang, Q., 2020. Determining effects of water and nitrogen input on maize (Zea mays) yield, water-and nitrogen-use efficiency: a global synthesis. Sci. Rep. 10, 1–12.
Liu, X.-Y., Koba, K., Makabe, A., Liu, C.-Q., 2014. Nitrate dynamics in natural plants: insights based on the concentration and natural isotope abundances of tissue nitrate. Front. Plant Sci. 5.
Marshall, T., Holmes, J., Rose, C., 1996. Soil Physics. Cambridge University Press, Cambridge, UK, pp. 274–307.
Molina, J., Clapp, C., Shaffer, M., Chichester, F., Larson, W., 1983. NCSOIL, a model of nitrogen and carbon transformations in soil: description, calibration, and behavior. Soil Sci. Soc. Am. J. 47, 85–91.
Molz, F.J., 1981. Models of water transport in the soil-plant system: a review. Water Resour. Res. 17, 1245–1260.
Naser, M.A., Khosla, R., Longchamps, L., Dahal, S., 2020. Characterizing variation in nitrogen use efficiency in wheat genotypes using proximal canopy sensing for sustainable wheat production. Agronomy 10, 773.
Nye, P.H., Tinker, P.B., 1977. Solute Movement in the Soil-Root System. vol 4. Univ of California Press.
Powlson, D., Hart, P., Poulton, P., Johnston, A., Jenkinson, D., 1992. Influence of soil type, crop management and weather on the recovery of 15 N-labelled fertilizer applied to winter wheat in spring. J. Agric. Sci. 118, 83–100.
Richards, L.A., 1931. Capillary conduction of liquids through porous mediums. J. Appl. Phys. 1, 318–333.
Robertson, G.P., Vitousek, P.M., 2009. Nitrogen in agriculture: balancing the cost of an essential resource. Annu. Rev. Environ. Resour. 34, 97–125.
Roderick, M., Sun, F., Lim, W.H., Farquhar, G., 2014. A general framework for understanding the response of the water cycle to global warming over land and ocean. Hydrol. Earth Syst. Sci. 18, 1575–1589.
Roose, T., Fowler, A., 2004. A mathematical model for water and nutrient uptake by plant root systems. J. Theor. Biol. 228, 173–184.
Roose, T., Fowler, A., Darrah, P., 2001. A mathematical model of plant nutrient uptake. J. Math. Biol. 42, 347–360.
Roques, S., Berry, P., Knight, S., Morris, N., Clarke, S., Sagoo, E., 2016. RB209 review and revision: WP4 cereals and oilseeds. AHDB Research Review Number 3110149017.
Ruiz, S., Fletcher, D.M., Boghi, A., Williams, K., Duncan, S., Scotson, C., et al., 2020a. Image-based quantification of soil microbial dead zones induced by nitrogen fertilization. Sci. Total Environ. 727, 138197.
Ruiz, S., Koebernick, N., Duncan, S., Fletcher, D.M., Scotson, C., Boghi, A., et al., 2020b. Significance of root hairs at the field scale–modelling root water and phosphorus uptake under different field conditions. Plant Soil 447, 281–304.
Ruiz, S.A., Mckay Fletcher, D., Williams, K., Roose, T., 2020c. Review of plant-soil modelling: root growth, nutrient and water transport/uptake, and mechanics. Annual Plant Reviews online.
Shackelford, C.D., Daniel, D.E., 1991. Diffusion in saturated soil. I: background. J. Geotech. Eng. 117, 467–484.
Sharp, R.E., Silk, W.K., Hsiao, T.C., 1988. Growth of the maize primary root at low water potentials: I. Spatial distribution of expansive growth. Plant Physiol. 87, 50–57.
Smith, J., Bradbury, N., Addiscott, T., 1996. SUNDIAL: a PC-based system for simulating nitrogen dynamics in arable land. Agron. J. 88, 38–43.
Snyder, C., Davidson, E., Smith, P., Venterea, R., 2014. Agriculture: sustainable crop and animal production to help mitigate nitrous oxide emissions. Curr. Opin. Environ. Sustain. 9, 46–54.
Stout, W., Fales, S., Muller, L., Schnabel, R., Weaver, S., 2000. Water quality implications of nitrate leaching from intensively grazed pasture swards in the northeast US. Agric. Ecosyst. Environ. 77, 203–210.
Tinker, P.B., Nye, P.H., 2000. Solute Movement in the Rhizosphere. Oxford University Press.
van Genuchten, M.T., 1980. A closed-form equation for predicting the hydraulic conductivity of unsaturated soils. Soil Sci. Soc. Am. J. 44, 892–898.
Walsh, O., Raun, W., Klatt, A., Solie, J., 2012. Effect of delayed nitrogen fertilization on maize (Zea mays L.) grain yields and nitrogen use efficiency. J. Plant Nutr. 35, 538–555.
Zhang, X., Davidson, E.A., Mauzerall, D.L., Searchinger, T.D., Dumas, P., Shen, Y., 2015. Managing nitrogen for sustainable development. Nature 528, 51–59.
Zhao, D., Reddy, K.R., Kakani, V.G., Reddy, V., 2005. Nitrogen deficiency effects on plant growth, leaf photosynthesis, and hyperspectral reflectance properties of sorghum. Eur. J. Agron. 22, 391–403.